This is the authors' version of the article published in Materials Advances were made to this version by the publisher prior to publication. The final version is available at https://doi.org/10.1021/acs.biomac.3c01261

Design of 3D-Photoprintable, Bio- and Hemocompatible Non-Isocyanate Polyurethane Elastomers for Biomedical Implants

Anna Pierrard[‡a], Sofia F. Melo[‡b,c], Quinten Thijssen[d], Sandra Van Vlierberghe[d], Patrizio Lancellotti[b,e], Cécile Oury[b], Christophe Detrembleur[a], Christine Jérôme[a]*

[‡]Authors contributed equally to this work.

[a] Center for Education and Research on Macromolecules (CERM), University of Liege (ULiege), CESAM-RU, Department of Chemistry, Sart-Tilman, Building B6a, B-4000 Liege, Belgium

[b] GIGA Cardiovascular Sciences - Laboratory of Cardiology, University of Liège, Avenue de l'Hôpital 11, Quartier Hôpital, Building B34, 4000 Liège, Belgium. E-mail: Cecile.Oury@uliege.be

[c] Faculty of Medicine, University of Liège, Avenue Hippocrate 15, Quartier Hôpital, 4000 Liège, Belgium.

[d] Polymer Chemistry and Biomaterials Group, Centre of Macromolecular Chemistry, Ghent University, Krijgslaan 281 S4, 9000 Ghent, Belgium.

[e] Department of Cardiology - Centre Hospitalier Universitaire (CHU) of Liège, University of Liège Hospital, Liège, Belgium

* Corresponding authors: **E-mail:** c.jerome@uliege.be

Abstract

Polyurethanes (PUs) have adjustable mechanical properties making them suitable for a wide range of applications, including in the biomedical field. Historically, these PUs have been synthesized from isocyanates which are toxic compounds to handle. This has encouraged the search for safer and more environmental-friendly synthetic routes, leading today to the production of non-isocyanate polyurethanes (NIPUs). Among these NIPUs, polyhydroxyurethanes (PHUs) bear additional hydroxyl groups, which are particularly attractive for derivatizing and adjusting their physico-chemical properties. In this paper, polyether-based NIPU elastomers with variable stiffness are designed by functionalizing the hydroxyl groups of a poly(propylene glycol)-PHU by a cyclic carbonate carrying a pendant unsaturation, enabling them to be post-photocrosslinked with polythiols (thiol-ene). Elastomers with remarkable mechanical properties whose stiffness can be adjusted are obtained. Thanks to the unique viscous properties of these PHU derivatives and their short gel times observed by rheology experiments, formulations for light-based 3D-printing have been developed. Objects were 3D-printed by digital light processing with a resolution

down to the micrometer scale, demonstrating their ability to target various designs of prime importance for personalized medicine. In vitro biocompatibility tests have confirmed the non-cytotoxicity of these materials for human fibroblasts. In vitro hemocompatibility tests have revealed that they do not induce hemolytic effects, they do not increase platelet adhesion nor activate coagulation, demonstrating their potential for future applications in the cardiovascular field.

Introduction

Polyurethanes (PUs) are one of the most produced polymers worldwide [1]. They are found in many diverse applications (flexible and rigid foams, adhesives, coatings, elastomers, …) thanks to their wide range of possible structures, which can give them very different properties [2]. This versatility is itself due to the wide choice of monomers available, i.e. isocyanates and polyols. One of the many advantages of PUs is their biocompatibility and biostability [1], which is due to their resistance to hydrolysis [3]. Therefore, PUs find various applications in the biomedical field, such as in drug eluting implants [4–6], catheters, blood oxygenators, or even scaffolds for tissue engineering [7,8]. Medical PU market size is forecasted to reach 5.2 billion U.S. Dollar by 2026, after growing 4.3% annually [9]. Especially, polyether-based PUs exhibiting elastomeric properties close to several natural tissues thanks to their soft polyether segments, and polycarbonate-based PUs showing long-term stability are particularly appealing even for highly demanding cardiovascular applications [10–14]. Currently, the industrial production of these PUs mainly relies on isocyanate chemistry which causes health issues such as lung injuries and asthma [15,16] and requires the handling of highly toxic compounds such as phosgene [17,18]. This historical process is no longer in line with the current evolution of regulations, such as European legislations of Registration, Evaluation, Authorization and Restriction of Chemicals (REACH) [19,20]. As a result, more environmental-friendly alternative synthetic routes are rapidly developing today to avoid the use of these reagents [21–25] and produce the so-called non-isocyanate polyurethanes (NIPUs).

An emerging green chemistry for the synthesis of NIPUs is the addition of an amine to a 5-membered cyclic carbonate [20,21,26]. The latter is less toxic than an isocyanate compound and is easily produced by the quantitative catalyzed coupling of CO_2 to an epoxide, making this process more eco-friendly [26–33]. NIPUs produced by this route hold primary and secondary hydroxyl groups along their backbone and are called polyhydroxyurethanes (PHUs) [34,35]. Segmented polyether-PUs, and notably poly(propylene glycol)-PUs (PPG-PUs) are exhibiting remarkable elastomer properties as well as a high biocompatibility which justifies their application in various medical devices, including in the highly demanding cardiovascular field. Therefore, efforts have been devoted to apply this green chemistry to the synthesis of PPG-PHU elastomers. Nevertheless, in this case, the hydroxyl groups of PHUs prevent the nanophase

separation that takes place in classic PPG-PUs (that exhibit thermoplastic elastomer properties), which alters the elastomeric behavior of PPG-PHUs, causing them to flow under the force of gravity. This effect is even more pronounced when PPG-PHUs are hydrated. Several groups have tried to restore the phase separation by incorporation of amide chain-extenders [36] or sterically hindered soft segments [37]. Some of us have also reported the crosslinking of PPG-PHU chains as a way to compensate for this loss of mechanical properties [38]. However, even though the hydroxyl groups affect the properties of these polyether-PHUs, they can also be advantageously used for the post-functionalization of PHUs and give them new properties and perspectives [39].

Since PHUs are relatively recent materials, biocompatibility studies are scarce in the literature. Degradable aliphatic polyester-PHUs were reported as biologically benign and used for drug delivery systems [40]. Cytotoxicity tests have demonstrated the biocompatibility of various PHU networks, such as bio-sourced tannic acid derived PHU networks [41] or aliphatic dihydroxyurethane crosslinked via thiol-ene [42] or via photopolymerization of acrylic groups [43]. As far as polyether-PHUs are concerned, the biocompatibility of poly(ethylene glycol) (PEG)-PHUs hydrogels was demonstrated. Being non cytotoxic, these hydrogels allow cells spreading and proliferation and are thus relevant for tissue engineering [44]. This is also the case for segmented PPG-poly(amide HU) electrospun as fibrous mats [45]. Finally, this green chemistry reaction of a cyclic carbonate with an amine was applied to link the blocks of the thermoresponsive PEG-HU-PPG-HU-PEG triblock copolymers, and hemocompatibility tests performed on the latter demonstrated that the hydroxy-urethane junction did not alter their hemocompatibility, showing the high potential of these NIPUs for cardiovascular applications [46].

In this work, we apply this new green chemistry approach, i.e., the reaction of an unsaturated CO_2-sourced cyclic carbonate with an alcohol [47] for the functionalization of a PPG-PHU in order to allow its post-photo-crosslinking. Therefore, we exploit an easily accessible CO_2-based 5-membered cyclic carbonate, namely αCC (see **Scheme 1**), for the preparation of PPG-carbonate-based NIPUs carrying pendant unsaturations. This modified PPG-NIPU is then photo-crosslinked in the presence of various polythiols, chosen to adjust the mechanical properties of the resulting elastomers, without the need to change the structure of the functionalized NIPU. Formulations are then developed to achieve their 3D printing by Digital Light Processing (DLP) (**Scheme 1**) to allow the customization of biomedical implants or prostheses. Finally, we assessed the biocompatibility of the materials by quantifying cytotoxic effects towards human primary fibroblasts in different *in vitro* assays. In addition, NIPUs hemocompatibility was also evaluated through the measurement of the hemolytic effects towards red blood cells (RBCs), the quantification of adhered platelets on NIPUs surfaces and the measurement

of clotting times upon contact with NIPUs. The latter demonstrated remarkable hemocompatibility, opening new opportunities for the design of blood-contacting drug eluting implants and prostheses for cardiovascular applications. This work therefore demonstrates that a new emerging green chemistry approach leads to NIPU elastomers with mechanical properties adaptable to various natural tissues, and which can be 3D printed to design bio- and hemocompatible implants.

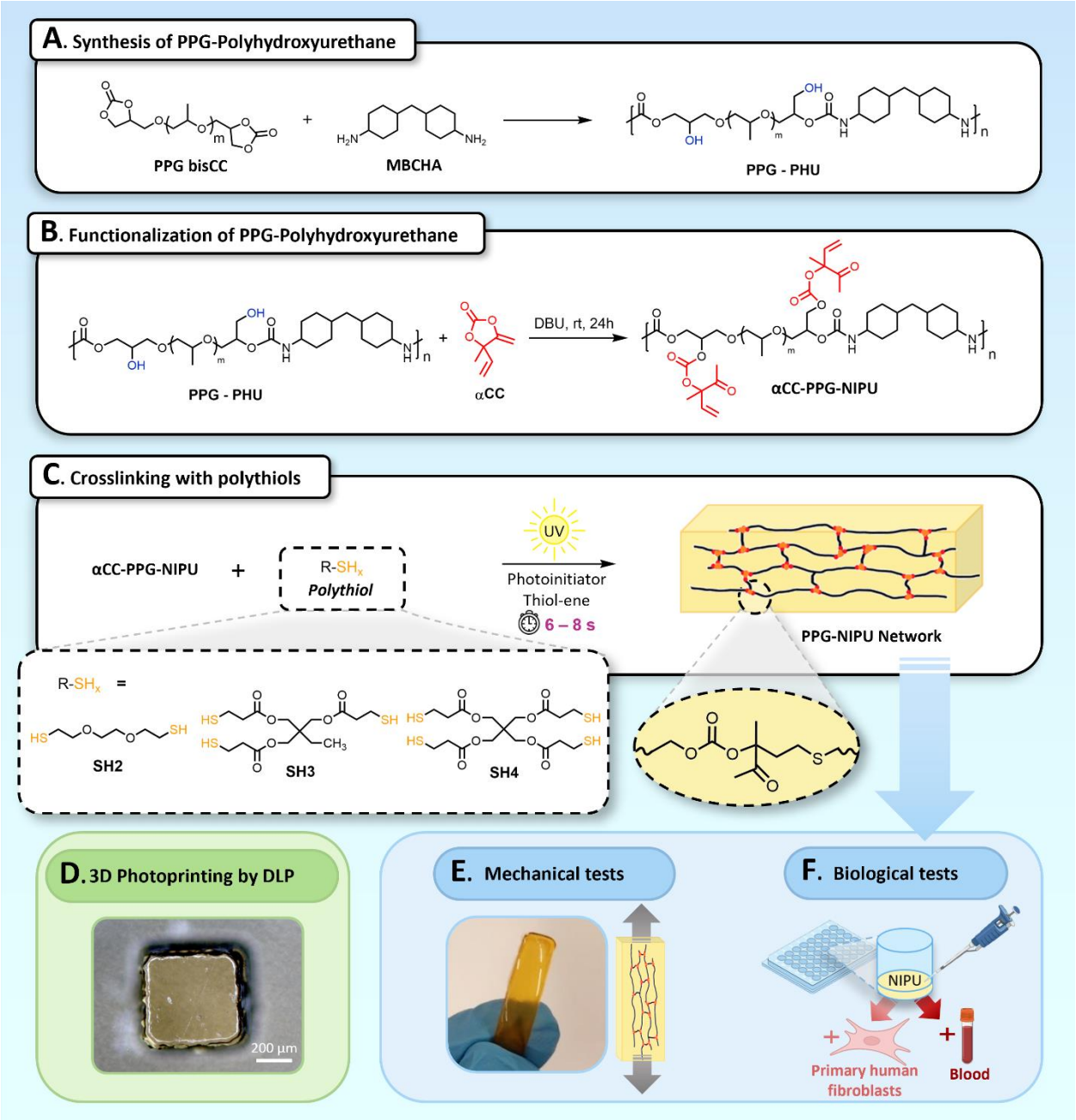

Scheme 1. Schematic illustration of the synthesis of the poly(propylene glycol)-polyhydroxyurethane (PPG-PHU) polymer precursor (A), functionalization of the hydroxyl groups of PPG-PHU by αCC (B), photo-crosslinking of αCC-PPG-PHU with a varying polythiol and a photoinitiator by a thiol-ene reaction (C), 3D printed PPG-NIPU-based object obtained by DLP (D), mechanical testing of the PPG-NIPU networks (E) and *in vitro* bio/hemobiocompatibility testing of the PPG-NIPU networks (F).

Experimental section

Materials

1-Methyl-2-pyrrolidone (NMP) (≥99.7%, Sigma-Aldrich), 1,8-diazabicyclo[5.4.0]undec-7-ene (DBU) (≥99%, Sigma-Aldrich), 2,2′-(Ethylenedioxy)diethanethiol (95%, Sigma-Aldrich), argon (Air Liquide), chloroform (≥99.8%, VWR Chemicals), CO_2 (N27) dimethylformamide (99.8%, DMF) (Acros), ethyl acetate (≥99.8%, Acros), Irgacure 819 (>95%, Ciba Specialty Chemicals Inc), pentaerythritol tetrakis(3-mercaptopropionate) (>95%, Sigma-Aldrich), trimethylolpropane tris(3-mercaptopropionate) (≥95%, Sigma-Aldrich), Carbothane™ (Lubrizol), Dulbecco's modified Eagle's medium (DMEM, Gibco, Thermo Fisher Scientific, USA), fetal bovine serum (FBS, Gibco, Thermo Fisher Scientific, USA), non-essential amino acids (NEAA, Gibco, Thermo Fisher Scientific, USA), amphotericin B (Gibco, Thermo Fisher Scientific, USA), penicillin/streptomycin (Pen/Strep, Biowest, France), phosphate buffered saline (PBS, Gibco, Thermo Fisher Scientific, USA), trypsin-EDTA solution (Gibco, Thermo Fisher Scientific, USA), Triton™ X-100 (Merck, USA), resazurin (10-oxido-7-oxophenoxazin-10-ium-3-olate, Stemcell Technologies, Canada), paraformaldehyde (PFA, Merck, USA), Phalloidin-Alexa Fluor® 488 (1:100, Molecular Probes), 6-diamidino-2-phenylindole dihydrochloride (DAPI, 3 µg/mL, Merck, USA), lactate dehydrogenase activity assay kit (LDH, Sigma-Aldrich, USA), CRYOcheck™ Pooled Normal Plasma (Cryopep, France), 5-CLOT NaPTT Reagent (NODIA, Belgium), $CaCl_2$ solution 1M (Merck, USA) were used as received without any further purification.

Characterization Methods

Fourier transformed infrared spectroscopy (FTIR). Fourier transform infrared spectra were recorded using a Nicolet IS5 spectrometer (Thermo Fisher Scientific) equipped with a diamond attenuated total reflectance (ATR) device. Spectra were obtained in transmission or ATR mode as a result of 32 spectra in the range of 4,000 – 500 cm^{-1} with a nominal resolution of 4 cm^{-1} and analyzed with an OMNIUM™ (Thermo Fisher Scientific) software.

Nuclear magnetic resonance spectroscopy (NMR). The samples were prepared by dissolving 20 mg of product in 650 µL of deuterated DMSO-d_6 or $CDCl_3$. ^1H- and HSQC (Heteronuclear single quantum coherence) NMR spectra were recorded at 298 K with a Bruker advance DRX 400 MHz spectrometer, in the Fourier transform mode.

Size exclusion chromatography (SEC). The number-average molecular weight (M_n), the weight-average molecular weight (M_w) and the dispersity (M_w/M_n) of poly(propylene glycol)-polyhydroxyurethanes were determined by size exclusion chromatography (SEC) in DMF containing LiBr (2.17 g/L) at 55 °C (flow rate: 1 mL/min) with a Waters chromatograph equipped with four columns (Waters Styragel HR 1, HR 3, HR4, HR5), a dual λ absorbance detector (Waters 2487) and a refractive index detector (Waters 2414.40 °C). A polystyrene calibration was used.

Tensile tests. The mechanical properties of the samples were realized at 25°C on a Q800 dynamic mechanical analyzer (DMA) from TA Instruments in DMA controlled force mode. Rectangular samples of 25×5×0.5 mm were tested and a starting distance of 7 mm between the clamps was chosen. For each sample, an equilibrium of 5 min at 25 °C was first applied, before starting to apply a force with a ramp of 0.05 MPa/min at 25 °C until breaking the sample. The data was analyzed with the software TRIOS™ (TA Instruments). The Young's modulus (E), the stress at break (σ) and the elongation at break (ε) of samples were calculated by averaging at least three reproductive values. Samples were analyzed in the dry state (after drying at 120 °C in an oven overnight) and in wet state (after immersion in water for 24h).

Swelling measurements. The swelling degrees of the networks were calculated by immersing each sample (previously weighed in dry state) in $CHCl_3$ at room temperature (average of at least three values). Measurements were taken every 30 minutes until the mass stabilized. They were determined by the following equation:

$$\text{Swelling degree} = (W_s - W_d)/W_d \times 100\%$$

where W_s is the weight of the swollen sample in $CHCl_3$ and W_d the weight of the dried sample before swelling.

Gel content measurements. The gel contents of the networks were calculated by comparing the weight of a sample in dry state before immersion in $CHCl_3$ (before swelling) and the weight of a sample after immersion for 24 hours in $CHCl_3$ at room temperature (swelling) and drying at 120 °C overnight (average of at least three values). They were determined by using the following equation:

Gel content = $W_{d,f}/W_d$ x 100%

Where $W_{d,f}$ is the weight of the sample dried at 120 °C overnight after immersion in $CHCl_3$ and W_d is the weight of the dried sample before swelling.

Equilibrium water absorption measurements (EWA). The equilibrium water absorptions of the networks were calculated by immersing each sample (previously weighed in dry state) in water at room temperature after 24 hours (average of at least three values). They were determined by the following equation:

Swelling degree = $(W_{s,w} - W_d)/W_d \times 100\%$

where $W_{s,w}$ is the weight of the swollen sample in water and W_d the weight of the dried sample before swelling in water.

Differential scanning calorimetry (DSC). The glass-transition temperatures were determined using a DSC 250 by TA Instruments with a baseline flatness ≤10 µW with a precision of ± 0.01°C. The procedure is the following: equilibration at -80 °C and isothermal step for 2 min (cycle 1), heating with a ramp of 10 °C/min up to 150 °C followed by an isothermal step for 5 min (cycle 2), equilibration at -80 °C and isothermal step for 2 min (cycle 3), heating with a ramp of 10 °C/min up to 200 °C (cycle 4). Thermograms were recorded during the fourth cycle and analyzed using the software TRIOS™ (TA Instruments).

Thermogravimetric analyses (TGA). Thermogravimetric analyses were performed on a TGA 2 model by Mettler Toledo with a weight precision of 0.005% and a resolution of 1 µg. The procedure is the following: samples were placed under air atmosphere (20 mL/min) and underwent a first heating from 30 to 100 °C, with a heating rate of 20 °C/min followed by an isothermal step at 100 °C during 10 min and finally a second heating from 100 up to 500 °C with a thermal ramp of 10 °C/min. The curves were analyzed using the STARe software.

Rheological measurements. The curing times of the formulations were determined by time sweep experiments performed on an ARES-G2 from TA Instruments equipped with parallel plate geometries (diameter of 25 mm, bottom in stainless steel, top in acrylic material transparent to UV). Interplate gaps of 0.1 mm were set, and the mixtures were deposited so that the geometries were completely filled. Normal forces were monitored to be relaxed before any measurement. A UV lamp Omnicure Series 2000 (200 W, wavelength = 365 nm) was used to illuminate the samples during the analyses and was turned on after 100 s of data collection (in order to reach an equilibrium). The procedure is the following: oscillation fast sampling during 200 s at 25 °C with a sampling rate of 1 pts/s, a strain of 1% and a frequency of 1 Hz followed by oscillation time during 300 s at 25 °C with a sampling interval of 2 s/pt, a strain of 1% and a frequency of 1 Hz. Flow sweep experiments were performed in order to measure the viscosity of the solutions using stainless steel parallel plate geometries (diameter of 25 mm) with gaps of 0.3 mm and 1% of strain at room temperature. The data was analyzed using the software TRIOS by TA Instruments.

Experimental Procedures

Functionalization of poly(propylene glycol)-polyhydroxyurethanes

Poly(propylene glycol)-polyhydroxyurethane (PPG-PHU) was prepared from carbonated poly(propylene glycol) diglycidyl ether and 4,4'-methylenebis(cyclohexylamine) (MBCHA) following a protocol described in ESI (**Figures S1-S5** and **Scheme 1.A**).[38,48,49] This yellow PPG-PHU (5 g, 0.025 mol of hydroxyl groups, 1 eq.) was then weighed in a 100 ml round bottom flask equipped with a magnetic stirrer. A minimal amount of dry DMF (20 mL) was added to the prepolymer under stirring until solubilization. Once the solubilization was complete, αCC (3.5 g, 0.025 mol, 1 eq.), synthesized following a protocol described in ESI (**Figures S6-7**) [49] and shown in **Scheme 1.B**, was added to the solution, followed by 1,8-diazabicyclo[5.4.0]undec-7-ene (DBU, 0.1903 g, 1.25 mmol, 0.1 eq.). The solution was placed under inert atmosphere and constant agitation for 24h. The brown solution was then purified by three successive precipitations: the product was precipitated in 300 mL of diethyl ether, centrifugated for 10 min at a speed of 10,000 min^{-1} at 15°C, resolubilized in 50 mL of $CHCl_3$ before being precipitated again (repeat the operation twice). The obtained brown functionalized polymer (αCC-PPG-NIPU, shown in **Scheme 1.B**) was then dried under vacuum. The quantitative functionalization of the alcohol functions (both primary and secondary) was checked by NMR and FTIR (**Figure S8-10**). A SEC analysis was also performed on the final product (**Figure S11**). M_w = 24,400 g/mol, M_w/M_n = 1.73 (PS calibration). **Figure S12** and **Figure S13** show the DSC and TGA curves of αCC-PPG-NIPU, respectively.

αCC-PPG-NIPU: ^{1}H-NMR (400 MHz, DMSO) δ (ppm) = 6.05 (dd, J = 17.5, 10.9 Hz, 1H), 5.48 – 5.24 (m, 2H), 4.91 (s, 1H), 4.35 – 3.99 (m, 2H), 3.84 – 3.09 (m, 49H), 2.09 (s, 3H), 1.85 – 0.70 (m, 19H).

Typical procedure for the synthesis of networks

In the following procedure (see **Scheme 1.C**), the molar ratios are calculated according to the number of moles of alkene functions present on the functionalized PHU determined by ^{1}H-NMR for each batch. Irgacure 819 (0.0974 mmol, 0.0407 g, 0.1 eq.) was weighed in a glass vial equipped with a magnetic stirrer before adding 100 µL of $CHCl_3$ to solubilize it under agitation away from UV light. Trimethylolpropane tris(3-mercaptopropionate) (SH3, 0.3214 mmol, 0.1281 g, 0.33 eq.) was then added, and the solution was stirred away from UV light. αCC-PPG-PHU (0.3 g, 0.9740 mmol of alkene, 1 eq. alkene *vs* thiol) was weighed in another glass vial equipped with a magnetic stirrer and solubilized in 1 mL of $CHCl_3$ by agitation. Once the solubilization was complete, the αCC-PPG-PHU solution was transferred to the vial containing the Irgacure 819 and the trithiol. The resulting solution was stirred and $CHCl_3$ was removed under vacuum away from UV light. The formulation was then poured in a Teflon mold (5 x 2.5 x 0.1 cm). The curing occurred by placing the mold under a UV lamp (Omnicure Series 2000, 200 W, Hg, wavelength = 365 nm) for 15 minutes. The mold was then placed at 120 °C in an oven for 24 hours to remove any remaining traces of $CHCl_3$. The resulting PPG-NIPU networks were then characterized by various techniques (see **Figure S14** for FTIR spectra, **Figure S15** for DSC curves and **Figure S16** for TGA curves). Networks synthetized starting from 2,2′-(ethylenedioxy)diethanethiol (SH2) and pentaerythritol tetrakis(3-mercaptopropionate) (SH4) were also prepared following this procedure by adapting the quantities of reagents (0.5 eq. and 0.25 eq. of thiols, respectively).

Procedure for the 3D printing of the PPG-NIPU SH3 formulation

The PPG-NIPU SH3 resin was chosen to conduct 3D printing experiments by digital light processing (DLP) in order to demonstrate the printability of the resin. The final formulation used for the trials was a solution with a concentration of 0.5 g of αCC-PPG-NIPU per mL of 1-methyl-2-pyrrolidone (NMP), a 1:3 molar ratio (0.33 eq.) of SH3 and 10 mol% of photoinitiator (Irgacure 819). No photoabsorber was used. The 3D printing trials were carried out at room temperature using a Lumen X 3D bioprinter by CELLINK working with a fixed wavelength of 405 nm, 100% of light intensity (corresponding approximatively to 48 mW/cm^2), an exposure time of 25 s per layer, a layer height of 50 µm, a first layer time scale factor of 1 and a build platform offset set to 0. These parameters are the result of a

first optimization, after trying different exposure times (between 20 and 30 s) and different first layer time scale factors (between 1 and 3). Each trial was made by pipetting 0.5 mL of solution in the center of a Petri dish (see **Figure 2.D** for the DLP printing experimental set-up). The computer-aided design (CAD) used for these printings is shown in **Figure S18.A** and is composed of 20 full layers (base) and 10 layers of cubic-like objects with varying dimensions (5×5 mm^2, 1×1 mm^2, 0.5×0.5 mm^2, 0.25×0.25 mm^2 and 0.1×0.1 mm^2). These objects were used to evaluate the resolution of the formulation chosen for the DLP process. Postprocessing of the printed objects included thoroughly washing with acetone and subsequent post-curing through photoirradiation for 10 min (using a UV lamp, Omnicure Series 2000, 200 W, Hg, wavelength = 365 nm). Pictures of the 3D printed objects were taken using a Zeiss Axiotech light microscope (see **Figure S18.B, C, D**, **E** and **F**).

Procedures for biological testing

1. *In vitro* biocompatibility: interactions with human fibroblasts

Primary cells and culture conditions. *In vitro* biocompatibility assays were performed using primary cultures of human fibroblasts. Cells were expanded in Dulbecco's modified Eagle's medium (DMEM) supplemented with 10% volume/volume (v/v) fetal bovine serum (FBS), 1% v/v non-essential amino acids (NEAA), 2,5 µg/mL of amphotericin B and 1% v/v penicillin/streptomycin (Pen/Strep) at 37 °C, in a humidified atmosphere, containing 5% v/v CO_2. Medium was refreshed every two days. When reaching 90% confluence, cells were rinsed with 5 mL of phosphate buffered saline (PBS) (37 °C) and detached from culture flasks using 2 mL of Trypsin-EDTA solution.

Indirect Contact (extracts). The cytocompatibility of the synthetized polymers was initially evaluated using the indirect contact assay, by incubation of the cells with extracts of the materials, which were prepared as described in ISO 10993−12:2004. Firstly, 5-mm polymer discs were thoroughly rinsed with NaCl 0.9% for 72 h at 37 °C with agitation (100 rpm). The NaCl solution was refreshed every 24 h. To prepare the extracts, the washed discs were sterilized under UV, and incubated with DMEM for 24 h at 37 °C in an orbital shaker at 100 rpm. Cells were seeded in 96-well plates at density of 1×10^5 cells/mL and kept in culture for 24 h at 37 °C with 5% v/v CO_2. After 24 h, when a cell monolayer was formed, the materials' extracts were added, according to ISO 10993-5:2009(E), and the cells were incubated for other 24 h. A solution of Triton (X-100) 0.1% v/v was used as positive control of *in vitro* cytotoxicity.

Direct Contact. Polymer discs (diameter of 5 mm) were thoroughly rinsed with NaCl 0.9% for 72 h at 37 °C with agitation (100 rpm). The NaCl solution was refreshed every 24 h and the washed discs were sterilized under UV. Cells were seeded in 48-well plates at density of 1×10^5 cells/mL and kept in culture for 24 h at 37 ºC with 5% v/v CO_2. After 24 h, when a cell monolayer was formed, the sterile polymer discs were added to each well, and the cells were incubated for other 24 h. A solution of Triton (X-100) 0.1% v/v was used as positive control of *in vitro* cytotoxicity.

Measurement of the metabolic activity. Metabolic activity of the fibroblasts was quantified using a resazurin-based assay. For that, culture medium was removed from the wells and fresh media containing 10% v/v resazurin was incubated with the cells for 4 h at 37 °C with 5% v/v CO_2. Afterwards, medium was transferred to a black 96-well plate and the relative fluorescence units (RFUs) were measured ($\lambda_{ex} \approx 530$ nm, $\lambda_{em} \approx 590$ nm) using a micro-plate reader. Results were displayed as a percentage of the negative control (metabolic activity of cells contacting with PU/PPG-NIPU relatively to cells in contact with DMEM alone). Statistically significant differences between PU and NIPUs were calculated through one-way ANOVA with Dunnett's multiple comparisons test.

Visualization of adherent cells. After 24 h of culture, the fibroblasts were rinsed with PBS, fixed using paraformaldehyde (PFA) 4% weight/volume in PBS for 15 min, rinsed again with PBS, and prepared for visualization by fluorescent microscopy using a confocal Nikon A1R hybrid resonant microscope. For that, cells were stained for the identification of deoxyribonucleic acid (DNA) and filamentous actin (F-actin), using 6-diamidino-2-phenylindole dihydrochloride (DAPI) in a concentration of 3 µg/mL, and phalloidin conjugated with Alexa Fluor 488 in a 1:100 dilution, respectively. Incubation with phalloidin was performed for 1 h in the dark, under mild agitation. After that, cells were rinsed with PBS and kept at 4 °C until confocal microscopy observation. DAPI was added approximately 10 min before microscopy imaging. Representative scanned z-series of the samples were projected onto a single plane and pseudo-colored using ImageJ software.

2. *In vitro* hemocompatibility: interactions with blood components

For hemocompatibility testing, blood samples from healthy donors who did not take any aspirin or anticoagulant in the last 20 days prior to the experiment were used. The study was approved by the Ethics Committee of the University Hospital of Liege, Belgium, and was performed in accordance with EU regulation on collection and use of samples of human body material for research purposes (Royal Decree and the provisions of the Act concerning biobanks entered into force on 1 November 2018, law 19/12/2008).

Hemolysis test (erythrocytes). *In vitro* hemocompatibility was firstly evaluated through hemolysis testing, using red blood cells (RBCs). Fresh human blood was collected from healthy donors into citrated tubes (3.8% sodium citrate), and the first tube was discarded to avoid tissue factor effects. Whole blood was centrifuged at 150xg for 15 min and platelet-rich-plasma (PRP) was removed. RBCs were re-suspended in PBS and centrifuged at 800xg for 10 min. RBCs were washed for another 2 times, or until the supernatant was clear, and a ratio of 1:7 RBCs/PBS was used for the test. The RBCs/PBS solution alone was used as negative control (CTL -). The synthetized polymers were cut into 5 mm (diameter) discs and thoroughly rinsed with NaCl 0.9% for 72 h at 37 °C with agitation (100 rpm). The NaCl solution was refreshed every 24 h. The washed discs were sterilized under UV, and incubated with the RBCs/PBS for 3 h at 37 °C in an orbital shaker at 100 rpm. Surface-area-to-volume ratios comply with ISO 10993-12, ISO 10993-4 and ASTM Standard F756-13. Using distilled water (dH_2O), a solution of RBCs/dH_2O (1:7) was prepared and used as positive control (CTL +) of hemolytic effect, since water is known to induce RBCs' lysis. After 3 h of incubation, the RBCs solutions were centrifuged at 800xg for 15 min, the supernatants were transferred to a 96-well polystyrene plate, and the absorbance was measured ($\lambda \approx 545$ nm) using a micro-plate reader. Absorbance values were compared to the positive and negative controls, and hemolysis rates were displayed in percentage. Statistically significant differences between PU and NIPUs were calculated through one-way ANOVA with Dunnett's multiple comparisons test.

Lactate dehydrogenase activity (platelet adhesion). Whole blood was centrifuged at 150xg for 15 min, PRP was collected, and platelets were counted. The desired concentration (250,000 platelets/µL) was obtained through dilution in platelet-poor plasma (PPP). The synthetized polymers were cut into 5 mm (diameter) discs and thoroughly rinsed with NaCl 0.9% for 72 h at 37 °C with agitation (100 rpm). The NaCl solution was refreshed every 24 h. The washed discs were sterilized under UV and incubated with PRP for 2 h at 37 °C in an orbital shaker at 100 rpm. After 2 h of incubation, adherent platelets were washed with PBS and subsequently lysed with Triton (X-100) 1% v/v. Lactate dehydrogenase (LDH) activity in the lysates was measured using a colorimetric assay kit from Sigma-Aldrich. Absorbance values ($\lambda \approx 450$ nm) were compared to positive and negative controls (platelet adhesion on glass coverslips and absence of platelets, respectively), and statistically significant differences between PU and NIPUs were calculated through one-way ANOVA with Tukey's multiple comparisons test.

Coagulation test (clotting time). PPP (CRYOcheck) was thawed at 37 ºC for 5 minutes. The synthetized polymers were cut into 5 mm (diameter) discs and thoroughly rinsed with NaCl 0.9% for 72 h at 37 °C with agitation (100 rpm). The NaCl solution was refreshed every 24 h. The washed discs were sterilized under UV and incubated with the PPP for 2 h at 37 °C in an orbital shaker at 100 rpm. PPP alone was used as negative control of

coagulation activation, while kaolin-coated glass coverslips were used as positive control. After 2 h of incubation, human plasma clotting time was measured through a non-activated partial thromboplastin time (NaPTT) test. NaPTT reagent (NODIA) was added to the PPP samples and incubated for 1 minute at 37 ºC. A solution of calcium chloride (0.025 M) was added to the pre-warmed samples, and clotting endpoints were measured using a STAR4 apparatus. Statistically significant differences between PU and NIPUs were calculated through one-way ANOVA with Dunnett's multiple comparisons test.

Results and discussion

Functionalization of PPG-PHU by αCC

For the synthesis of elastomers, which is visible in **Scheme 1**, a CO_2-based α-alkylidene cyclic carbonate (αCC, bearing a pendant olefin) was used for the modification of the hydroxyl groups of a poly(propylene glycol)-based polyhydroxyurethane (PPG-PHU). The latter was synthesized by the solvent- and catalyst-free polyaddition of poly(propylene glycol)-bis(cyclic carbonate) (PPG bisCC, synthesized from a 380 g/mol PPG-diglydicyl ether precursor) with 4,4'-methylenebis(cyclohexylamine) (MBCHA) at 70 °C for 96 h, as already reported in the literature [38,48]. The structure of this viscous polymer was confirmed by NMR and FTIR spectroscopy (see ESI for details; **Figures S1a** (^{1}H-NMR)**, S1b** (HSQC-NMR) and **S2** (FTIR-ATR)) and its molecular characteristics were assessed by size exclusion chromatography calibrated by polystyrene standards (M_w = 16,100 g/mol, M_w/M_n = 2.2, see **Figure S3**). The hydroxyl groups (both primary and secondary) of the polymer backbone were then reacted by the αCC to deliver the functionalized NIPU as illustrated on **Scheme 1.B**. This cyclic carbonate, which carries two unsaturations, was selected for its high reactivity towards alcohols thanks to the exocyclic C=C bond that activates the opening of the cyclic carbonate [47]. Therefore, this reaction occurs efficiently at room temperature in the presence of a superbase as catalyst (1,8-diazabicyclo[5.4.0]undec-7-ene, DBU, 10 mol%) without any side reaction or by-products [47,50,51], and leads to the oxo-carbonate functionalized PPG-NIPU (αCC-PPG-NIPU). This is also a greener substitute to toxic phosgene commonly used as carbonylating agent for the preparation of carbonates from alcohols. Under these operating conditions, the quantitative functionalization of both primary and secondary alcohols into carbonate moieties bearing C=C double bonds was achieved, as evidenced by NMR and FTIR analyses. As shown in **Figure S8a & b**, the peaks corresponding to the functionalization by the αCC are clearly visible, i.e., q (CH_3 at 1.52 ppm), r (CH at 6.10 – 6.00 ppm), s (CH_2 at 5.43 – 5.27 ppm) and t (CH_3 at 2.09 ppm), as well as the

neighboring peaks n (CH_2 at 4.35 – 3.99 ppm) and o' (CH at 4.99 – 4.89 ppm). The similar neighboring peaks of the alcohol groups present on the PPG-PHU precursor have completely disappeared, as shown in **Figure S1a & b** and in the stacking of the ^{1}H-NMR spectra in **Figure S9**, such as the peaks b' (CH of the secondary alcohols at 4.73 – 4.59 ppm), a (CH_2 next to the secondary alcohols at 4.02 – 3.80 ppm), and g (CH_2 of the primary alcohols at 3.53 – 3.41 ppm), which therefore prove the complete functionalization. The integrals are also in agreement with the targeted structure. All assignments are confirmed by HSQC-NMR study (**Figure S8b**). The functionalization was also confirmed by FTIR (**Figure S10**), by the decrease of the C=C vibration bands (~ 1,680 – 1,640 cm^{-1}), the disappearance of the typical band of the cyclic carbonate, i.e., C=O stretching mode (~ 1,820 cm^{-1}) (visible in **Figure S7**), and appearance of the bands corresponding to CH_3-CO~ at ~ 1,795 cm^{-1}. The bands in the range ~ 3,500-3,200 cm^{-1} also decrease, due to the disappearance of the hydroxyl groups, the N-H stretching mode only remaining in this area. Other bands include C=O (chain-ends, ~ 1,795 cm^{-1}), O-CO-O (~ 1,740 cm^{-1}), and C-O-C of the PPG ether segments (~ 1,080 cm^{-1}). The size exclusion chromatography analysis of the viscous functional αCC-PPG-NIPU showed a M_w = 24,400 g/mol with M_w/M_n = 1.73 (**Figure S11**).

The yellow and brown colors observed for the PHU precursor and the functional NIPU, respectively, are most likely due to the oxidation of the amine end-groups into strongly colored oxides. This would prevent applications where strictly colorless materials are mandatory which is rarely the case for biomaterials.

Syntheses and properties of the PPG-NIPU elastomers

We then studied the ability of the functional NIPU (αCC-PPG-NIPU) to cure under UV light in the presence of a polythiol as a crosslinker and a photoinitiator (Irgacure 819, 0.1 molar eq.), the two quantities of which were calculated according to the number of moles of alkene functions present on the αCC-PPG-NIPU determined by ^{1}H-NMR. Three polythiols were tested in order to evaluate their influence on the properties of the final elastomers. Therefore, either a di- (SH2), tri- (SH3) or tetrafunctional (SH4) polythiol was used (see **Scheme 1.C.** for their structures), all of them being commercially available and added to get a stoichiometric amount of thiol functions towards NIPU unsaturations. The gel time of these three different formulations was assessed by rheology through time sweep experiments conducted at 25 °C (**Figure 1.A, B & C**). In each experiment, parallel plates were used, one of them being transparent to UV light (λ = 365 nm), which was turned on after 100 s of equilibration. Before UV irradiation, the NIPU-crosslinker mixture is viscous as shown by the loss moduli (G") dominating the storage moduli (G'). As soon as the irradiation started, both G' and G" rapidly increased and crossed after short and similar

gel times, i.e., around 6 to 8 s, showing the network formation that is here photo-induced by thiol-ene addition. The storage moduli reached a plateau with values up to ~ 8,000 Pa (with SH2), 55,000 Pa (with SH3) and 58,000 Pa (with SH4), indicating that the crosslinking density increases with the crosslinker functionality, as expected.

In order to investigate the crosslinking efficiency and the impact of the crosslinker functionality on the material properties, the three formulations (containing αCC-PPG-NIPU, one of the polythiols and the photoinitiator) were poured in a flat Teflon mold and irradiated with the same UV lamp as used for the rheological measurements (λ = 365 nm, 2,000 W) for 15 min. Prior to demolding, the networks were exposed to 120 °C for 24 h to remove any remaining traces of chloroform before being characterized by various techniques. The FTIR-ATR spectra of the networks are shown in **Figure S14.**

Swelling tests in chloroform (a good solvent for PPG) were conducted to characterize the network formation and revealed that the swelling was strongly dependent on the type of polythiol used, and therefore on the network crosslinking density. Indeed, a high swelling value (349.7%), due to limited crosslinking, was obtained for the network formed with the dithiol SH2. This value strongly decreased for SH3 and went down to 123.8% for the tetrathiol SH4, as a result of a higher crosslinking density (see **Table 1**). High gel contents (above 90%) were measured for the SH3 and SH4 formulations, showing the efficiency of the reaction performed for 15 min. In case of difunctional thiol (SH2), the gel content of 63% conveys the lower crosslinking capacity of the difunctional crosslinker keeping still soluble a third of the sample after 15 min of irradiation.

Table 1: Properties of the PPG-NIPU networks formed with SH2, SH3 or SH4 crosslinkers (measured at 25 °C).

Entry	Thiol	Swelling in $CHCl_3$ (%)	Gel Content (%)	EWA (%)	T_g (°C)	Mechanical Properties (dry)			Mechanical Properties (wet)		
						E (MPa)	σ (MPa)	ε (%)	E (MPa)	σ (MPa)	ε (%)
1	**SH2**	349.7 ± 39.3	63.1 ± 0.9	4.2 ± 0.5	7.9	2.4 ± 0.6	0.9 ± 0.09	108.6 ± 1.3	1.8 ± 0.2	0.5 ± 0.1	52.4 ± 1.9

2	**SH3**	195.2 ± 28.1	90.2 ± 0.2	4.0 ± 2.1	24.9	5.2 ± 1.4	1.1 ± 0.03	82.2 ± 0.3	3.7 ± 1.3	0.8 ± 0.2	43.5 ± 2.1
3	**SH4**	123.8 ± 0.3	98.6 ± 0.8	3.2 ± 0.08	42.4	16.0 ± 1.0	1.1 ± 0.1	40.8 ± 0.05	9.0 ± 2.2	0.8 ± 0.4	21.8 ± 4.1

Equilibrium water absorption (EWA) measurements showed relatively similar low water absorption values for the different networks (4.2, 4.0 and 3.2% with SH2, SH3 and SH4, respectively) due to the hydrophobic behavior of the PPG segments. We should point out that the water absorption also decreases when the crosslinking density increases, which is in line with our expectations. This limited swelling in water, due to the functionalization of the hydrophilic alcohol groups by the hydrophobic carbonate moieties, and followed by the additional crosslinking of the chains, is particularly important and desired in the case of biomaterials in contact with the human body such as implants in order to preserve their properties since they are subject to hydration.

The variation of the crosslinking density brought by the use of the different crosslinkers deeply impacts the glass transition temperatures (T_g's) of the networks. Differential scanning calorimetry (DSC) analyses of the networks (**Figure S15**), show a clear increase of the T_g's, from 7.9 °C (for SH2) to 24.9 °C (for SH3), and to 42.4 °C (for SH4) (see **Table 1**), which is in line with the increased crosslinking degree and consequently the decrease of chain segment mobility. While the T_g of the SH2 network remains low, the T_g of the SH4 network is shifted slightly higher than the body temperature. Thermogravimetric analyses (TGAs) were also conducted on the materials (see **Figure S16**) and showed thermal degradation temperatures of 10% ($Td_{10\%}$) at 217 °C (for SH2), 190 °C (for SH3) and 185 °C (for SH4). These values are similar to those obtained before ($Td_{10\%}$ = 224 °C) and after functionalization ($Td_{10\%}$ = 187 °C) of the PPG-PHU precursor, which shows that the post-functionalization reaction does not promote faster thermal degradation.

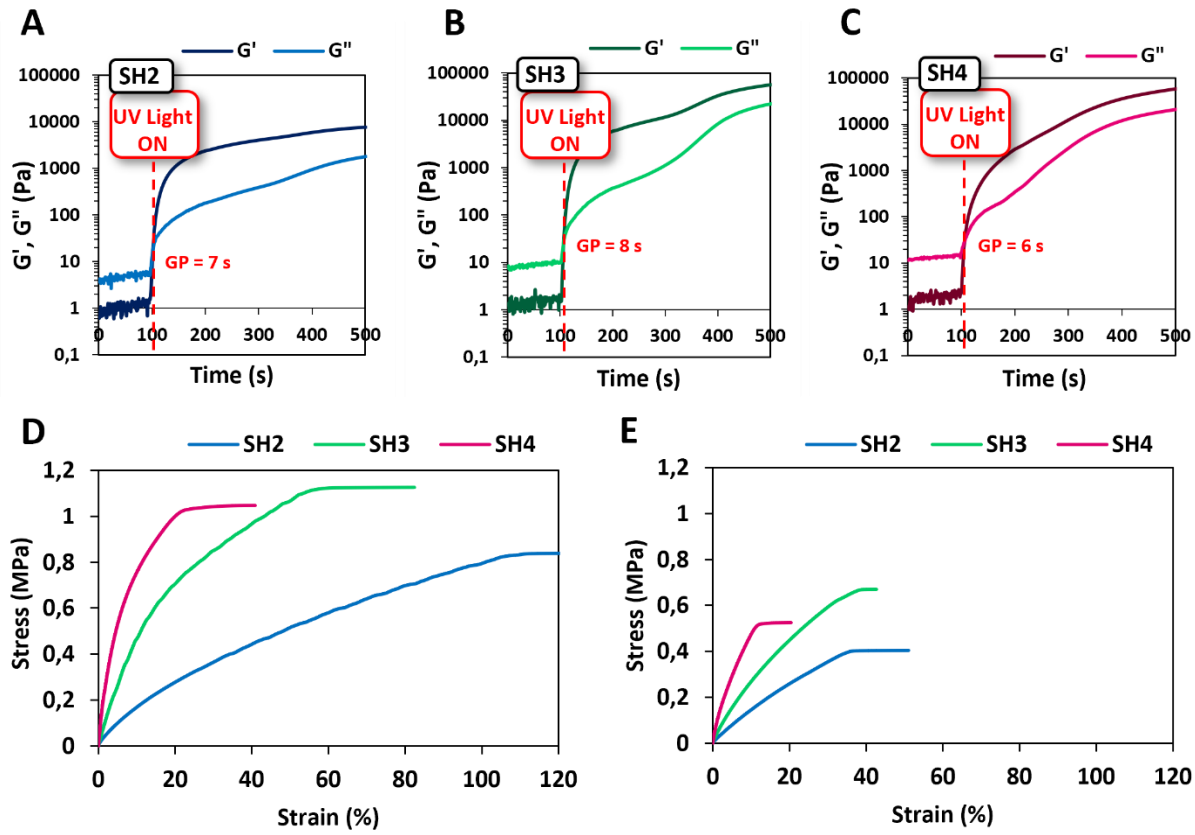

Figure 1: Evolution of the storage (G') and loss (G") moduli vs. time of the formulations with SH2 (A), SH3 (B) and SH4 (C) under UV irradiation (on after 100 s). Example of stress-strain curves of the PPG-NIPU networks formed with SH2, SH3 and SH4 in dry (D) and hydrated (E) state.

Finally, the mechanical properties of the networks were assessed by performing tensile tests on rectangular samples of material (25×5×0.5 mm^3) using a dynamic mechanical analyzer (DMA). These analyses were performed in the dry (**Figure 1.D**) and wet state (after immersion of each sample in water for 24 h, **Figure 1.E**) in order to observe the impact of hydration on the mechanical properties, considering further biomedical application as an implanted prosthetic material which would be constantly exposed to physiological fluids. The impact of the type of crosslinker on the mechanical properties of the networks was also directly visible. In the dry state, the Young's Modulus (E) increased from 2.4 MPa for (with SH2), to 5.2 MPa (with SH3) to even 16.0 MPa (with SH4), showing a huge variation in terms of material stiffness, which is in line with the measurements performed above or below the T_g of the networks. The stress at break (σ) remained interestingly constant, varying from 0.9 to 1.1 MPa, contrary to the elongation at break (ε), which varied from 108.6% (SH2) to 82.2% (SH3) and 40.8% (SH4), thereby showing a

reduction of more than a factor 2 between the crosslinking agent carrying 2 and 4 thiol functions. These results therefore also highlight the crosslinking density variation between samples. The same tendencies were observed in the wet state, the Young's Moduli varying from 1.8 to 3.7 to 9.0 MPa for the networks formed with SH2, SH3 and SH4, respectively. We can therefore observe lower values than in the case of the measurements in the dry state. If water plasticizing effect was already observed and reported for other NIPU-based materials (i.e., in foams and coatings) [52–55], in the present case, the PPG (polyether) based networks are swelling in water by 3 to 4 % (Table 1, EWA) which accounts for this decrease of the mechanical properties. The elongations at break in the dry state are for example divided by a factor 2 when changing to the wet state. However, even with the hydration impact, the mechanical properties of these networks remain attractive for potential uses as biomaterials. Indeed, different biomedical applications can be envisioned. Implantable materials such as synthetic vascular grafts or heart valve leaflets can be fabricated with these PPG-NIPUs to replace the native tissues. The SH2-based network shows for example mechanical properties close to those of human carotid artery, which has a E = 2.4 MPa, a σ = 0.95 MPa, and an ε = 105% (longitudinal measurements) [56,57]. Native heart valve tissues when considering the radial orientation show E = 2 MPa, σ = 0.4 MPa and ε = 30%, which are close to the values measured for SH3 [58,59]. The SH3-based network therefore shows great potential to be used for instance as biomaterial for new prosthetic heart valves. Lastly, the properties of the SH4-based network resemble those of human femoral arteries, which have much higher E values (9 MPa) but are not as demanding in terms of ultimate tensile strength and strain: 1 MPa and 63%, respectively (circumferential measurements) [60,61].

3D printing by digital light processing

In order to demonstrate the light-mediated 3D-printability of the NIPU-based formulations developed as above, Digital Light Processing (DLP) was selected. This 3D printing technique consists of a digital mirror device (DMD) to create 2D projections that selectively cure the photocurable resin layer-by-layer to build an object (**Figure 2.A**). DLP was chosen to illustrate this proof of concept due to its high resolution (between 25 and 150 µm), superior to that of extrusion-based techniques [62,63]. In order to adjust the viscosity of the PPG-NIPU/crosslinker formulations, a solvent was added to the mixture. As high boiling point solvent are required for DLP to avoid evaporation during the printing process, 1-methyl-2-pyrrolidone (NMP) was selected. Additional rheological experiments were therefore performed first to determine the amount of NMP to add to the mixture. The viscosity of solutions of different concentrations was measured by flow sweep experiments (see **Figure S17**). A concentration of 0.50 g of αCC-PPG-NIPU/mL was

eventually chosen, as it exhibited a viscosity of 0.13 ± 0.005 Pa.s, well below 10 Pa.s, generally referred to as the maximal viscosity value suitable for DLP [64]. This value also represents a good compromise between several factors, such as the ease of solubilization, a sufficient flow to replenish each new printed layer, and forces between the solution and the printed part which are not too strong in order to prevent the printed part from falling into the resin bath during printing. Time sweep experiments were then performed under UV irradiation with the same formulations containing NMP and 10 mol% of Irgacure 819 (photoinitiator). Gel points of 11 s (for SH2), 7 s (for SH3) and 5 s (for SH4) (**Figure 2.B, C** and **D**, respectively) were determined and demonstrate that the addition of NMP to the formulations does not delay the formation of the networks. Both the starting viscosity and the gel times of these formulations are therefore suitable for DLP even though the direct correlation between gel points and curing times when printing by DLP should be considered with caution as these rheological results were obtained using a 365 nm UV irradiation while the DLP machine is working with a 405 nm LED light source. A computer-aided design (CAD) was defined with parts featuring dimensions decreasing from 5 mm to 0.1 mm in order to show the resolution limit (along the X-Y axis) associated with the printing process (**Figure S18.A).** The final printing parameters are detailed in the materials and methods section. The morphology and dimensions of the collected 3D printed objects (whose dimensions varies from 5×5 mm^2 down to 129×143 μm^2) were measured either by vernier scale (for the 5×5 mm^2) or optical microscopy images, as shown in **Figure 2.A** and **Figure S18.B, C, D, E** and **F**. The correlations between theoretical and experimentally obtained determined sizes in the X-Y plan are visible in **Table S1** and show that the printed objects reproduce with very high fidelity the CAD model. It should be noted that the printing parameters can still be subject to future optimizations and that NMP, considered as a class 2 solvent by the Food and Drug Administration (FDA) [65], can be removed from the 3D printed object post-printing by several washing steps or successive swelling/drying of the networks. These results therefore show the suitability of these NIPU formulations to be 3D printed with sufficient resolution to foresee the precise design of small size devices such as implants or prosthesis requiring high definition (i.e., heart valve leaflet) [66].

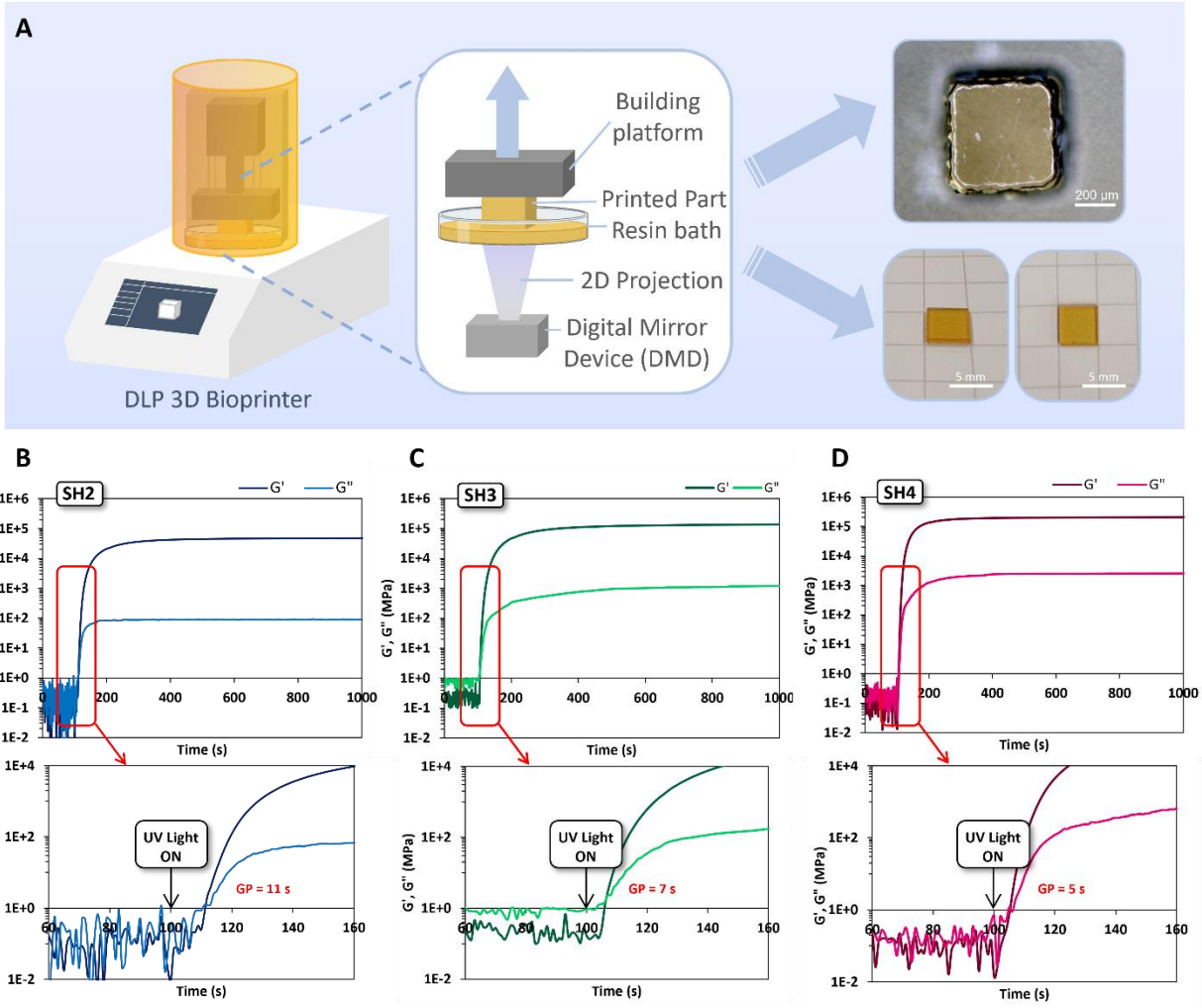

Figure 2: Scheme of the DLP printing process and pictures of successfully printed micro- and millimeter-scale cubic-like objects with the PPG-NIPU SH3 resin (A). Evolution of the storage (G') and loss (G") moduli vs. time of the formulations with SH2 (B), SH3 (C) and SH4 (D) in NMP.

Biological tests

For biological testing, medical grade PU (Carbothane^{TM}) was used as our reference of clinically used material.

***In vitro* biocompatibility: interactions with human fibroblasts**

According to ISO 10993, materials that are intended to be used as medical devices (or one of its components), which will come into direct or indirect contact with the human body, should be evaluated biologically to determine their potential *in vitro* cytotoxicity. For novel materials (i.e., materials that have not previously been used in a marketed medical device), it is recommended that both direct contact and extracting methods are considered.

Indirect Contact (extracts)

PU/PPG-NIPUs extracts were prepared by incubation of PU/PPG-NIPU discs with DMEM for 24 h at 37 ºC, under mild agitation (100 rpm). The extracts were then added to a monolayer of human fibroblasts in culture, which were incubated for another 24 h. Incubation with Triton (X-100) 0.1% v/v and DMEM alone were used as CTL + and CTL - of cytotoxicity, respectively. Cells were evaluated after the indirect contact (**Figure 3.A**) and fluorescence measurements based on a resazurin-assay revealed similar metabolic activities after contact with all materials extracts as with DMEM alone. According to ISO 10993-5:2009(E) [67], a threshold of 70% in the activity percentages (comparing to CTL -) should be set to consider a material as non-cytotoxic. Our results revealed percentages of 86%, 98% and 88% after contact with extracts of PPG-NIPUs with SH2, SH3 and SH4, respectively. This indicates that the leaching products of the polymer discs were not cytotoxic. As for extracts prepared from PU, the metabolic activity was 95%, which is in the same range of the percentages obtained for PPG-NIPUs' extracts. When looking into other studies interested in cytotoxicity evaluation of PU-derived materials, it was shown by different authors that it is possible to produce biocompatible membranes/scaffolds from a wide range of starting materials. Calvo-Correas *et al.* [68] showed that PUs prepared from poly(butylene sebacate)diol, ethyl ester L-lysine diisocyanate and 1,1,1-tris-(hydroxymethyl)propane have a non-toxic behavior. The viability analysis performed in the first 24 h revealed cell viability values around 90% (compared to the negative control), higher than the acceptance limit of 70%. Also Valdés *et al.*[69] proved that synthetized PU-based materials (different combinations of poly(propylene glycol), D-isosorbide, 4,4′-methylenebis(cyclohexyl isocyanate), and isophorone diisocyanate) exhibit low cytotoxicity towards human skin cells. In that study, cell viability (after 72 h of exposure) was evaluated by 3-(4,5-dimethylthiazol-2-yl)-2,5-diphenyltetrazolium bromide (MTT) reduction assay and revealed percentages above 80% for all tested samples. Our results, shown in **Figure 3.A,** add to the observations of other authors, and allow us to draw an optimistic conclusion, since the fibroblasts metabolic activities were > 85% after incubation with all PPG-NIPUs extracts, similar to the percentages obtained for extracts of medical grade PU. **Figure 4.A** shows representative confocal microscopy images of the same fibroblasts, where it is possible to observe that cells adhered and proliferated in the wells during the 24 h of incubation with the extracts. DNA was stained in blue with DAPI, while

F-actin was selectively stained in green using phalloidin-Alexa Fluor 488. Fibroblasts display their normal morphology, with evident F-actin stretching and spindle-like shape, in all the conditions evaluated (PU, PPG-NIPUs and DMEM). This corroborates the trends observed on the metabolic activity measurements.

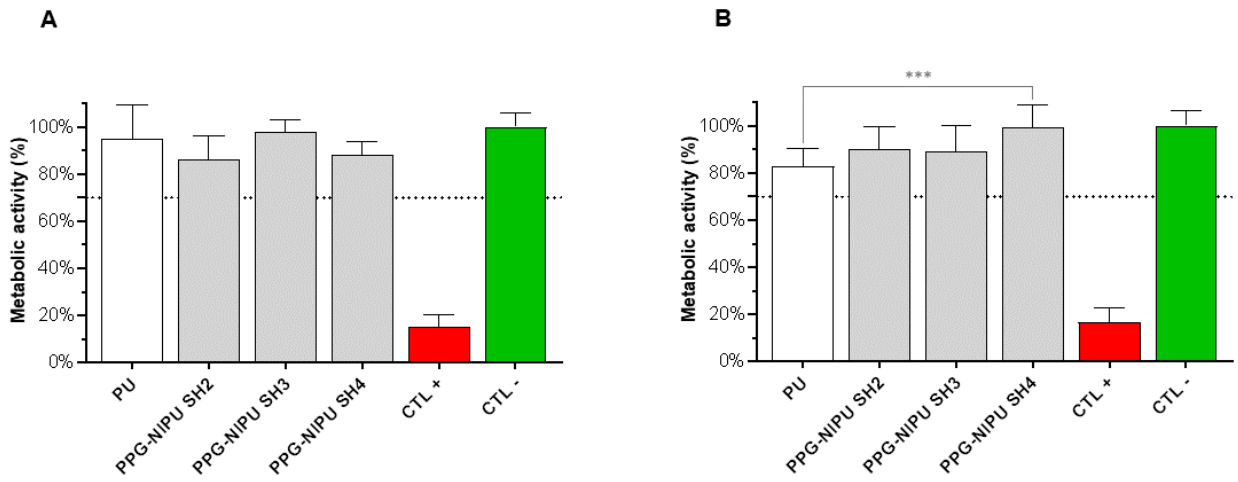

Figure 3: Metabolic activity of primary human fibroblasts after 24 h of indirect contact with PU/PPG-NIPUs, assessed by a resazurin-assay (A). Metabolic activity of primary human fibroblasts after 24 h of direct contact with PU/PPG-NIPU discs, assessed by a resazurin-assay (B). A solution of Triton (X-100) 0.1% v/v was used as positive control of in vitro cytotoxicity, while DMEM was used as negative control. Statistically significant differences between PU and NIPUs were computed using one-way ANOVA (***: adjusted p value < 0.001).

Direct Contact

In the direct contact assays performed to confirm the compatibility of the materials with the normal growth of human cells, the same primary fibroblasts were used. Cells were seeded and, once a monolayer was formed, they were put in direct contact (covered) with PU/PPG-NIPUs discs and cultured for another 24 h. The metabolic activity was monitored, and the results (**Figure 3.B**) confirmed that the polymer discs were non-cytotoxic. 90%, 89% and 99% were the activity percentages found for PPG-NIPUs with SH2, SH3 and SH4, respectively, expressed relatively to the CTL - (DMEM alone). The metabolic activity of cells in contact with PPG-NIPU SH4 (99%) was higher than of those that were in contact with PU (83%) ($p < 0.001$). This represents an interesting finding, since we show that PPG-NIPUs performed better than PU, which is widely described as an enhancer of cell growth and proliferation [70–72]. It was therefore shown that our materials are highly

biocompatible *in vitro*. Other authors demonstrated that direct contact of cells with PU-derived material surfaces was harmless, allowing cells to grow and proliferate. Bonfil *et al.* [73] showed cytocompatibility of castor oil and poly(ethylene glycol)-based polyurethane films, in which hexamethylene diisocyanate and 1,4-butane diol were used as diisocyanate and chain extender, respectively. In this study, the polymers did not induce cytotoxicity, with proliferation ratios of more than 80% for a murine fibroblast cell line (NIH 3T3) precultured for 24 h. Also Duarah *et al*. [74] evaluated the survival of primary human dermal fibroblasts cultured in polymer membranes of hyper branched biodegradable PU. No cell death was observed after 7 days of culture in all the studied membranes, suggesting materials' biocompatibility. Our results point at the same direction, in this case for NIPUs, and were confirmed by visual inspection of the cells, using confocal microscopy (**Figure 4.B**). The cells survived in the wells throughout the 24 h of culture in direct contact with the polymer discs. The observation of the preserved morphology of the cells, combined with the high percentages of metabolic activity found for the fibroblasts in direct contact with PPG-NIPUs, allow us to point out NIPUs as potentially implantable biomaterials, harmless to human fibroblasts, thus fulfilling the biocompatibility requirements.

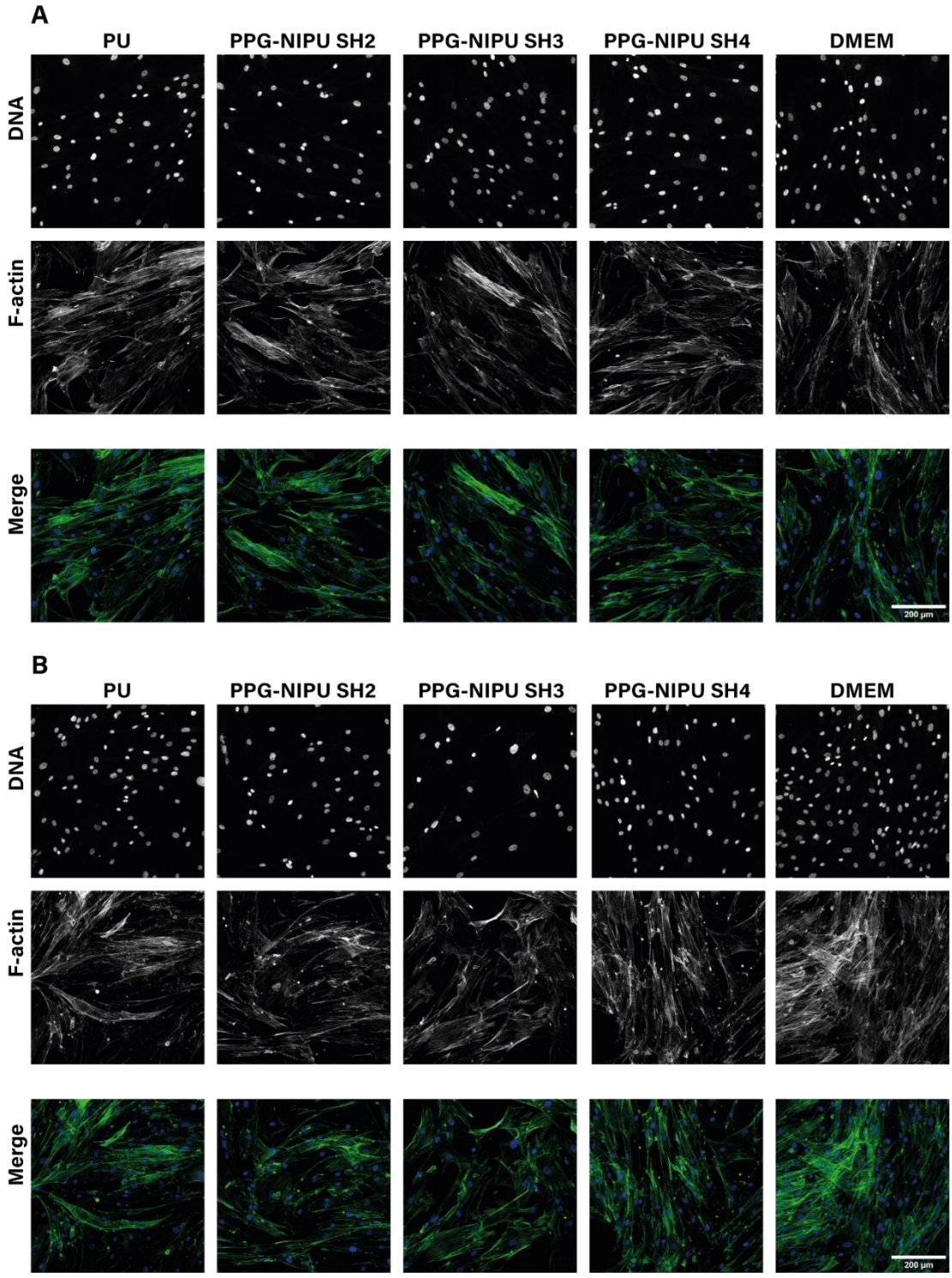

Figure 4: Fibroblasts morphology after 24 h of incubation with PU/PPG-NIPUs extracts and DMEM. Images represent projections of at least 50-µm height z-stacks. Scale bar: 200 µm (A). Fibroblasts morphology after 24 h of direct contact with PU/PPG-NIPUs discs

and DMEM. Images represent projections of at least 50-µm height z-stacks. Scale bar: 200 µm (B).

***In vitro* hemocompatibility: interactions with blood components**

In case of use of these materials in blood-contacting applications, these materials must exhibit hemocompatibility. Today, very few studies if any have focused on the hemocompatibility of NIPU-based biomaterials. The hemocompatibility of our different PPG-NIPU-based materials was evaluated through hemolysis tests (**Figure 5.A**) by incubating discs of the different elastomers with human RBCs. The *Standard Practice for Assessment of Hemolytic Properties of Materials* [75] describes 3 different categories: hemolytic materials, with a percentage of hemolysis greater than 5%; slightly hemolytic materials, with a hemolytic index between 5% and 2%; and non-hemolytic materials, with the hemolysis percentage below 2%. According to these criteria, all PPG-NIPUs (with SH2, SH3 and SH4) were non-hemolytic (with hemolysis rates of 0.3%, 0.2% and 0%, respectively), similar to our PU reference. These results revealed that all the produced PPG-NIPUs are harmless to RBCs, thus apparently safe for blood-contact applications. Other authors have described a wide range of hemolytic/non-hemolytic behaviors of PU-derived materials. Mystkowska *et al.* [76] found that the tested samples (different poly(ester-carbonate-urea-urethane)s produced from diisocyanates) had variable hemolytic effects, ranging from 3% to 10%. One of the materials, PACD-51-IPDI, derived from an oligo(pentamethylene adipate-co-carbonate), induced a much higher hemolysis rate (35%). On the other hand, Zhu *et al*. [77] observed that for all PUs - in this case produced using poly(1,6-hexanediol)carbonate diols as the soft segment and 4,4′-methylenebis(cyclohexyl isocyanate), 1,6-hexamethylene diisocyanate and 1,4-butanediol as the hard segment - the hemolysis rates were relatively low, always < 5%. Indeed, when compared to most studies evaluating PU-derived materials, all compositions of the PPG-NIPU-based materials here described show extremely low hemolysis rates and are therefore promising candidates to be used in the manufacturing of blood-contacting devices.

Platelet adhesion on the material surfaces (**Figure 5.B**) was evaluated in LDH assays, after incubating the PU/PPG-NIPUs discs with PRP for 2 h. Glass coverslips were used as CTL +, promoting platelet adhesion. The mean value of absorbance for glass was 1.18, while it was much lower for PU, PPG-NIPU SH2, PPG-NIPU SH3 and PPG-NIPU SH4 (0.23, 0.32, 0.36 and 0.45, respectively). This indicates very low levels of platelet adhesion on the surface of all tested elastomers. Nevertheless, we observed more platelet adhesion on PPG-NIPU SH4 than on other NIPUs and PU.

Contact activation of the coagulation cascade was studied in human PPP upon incubation (2 h) with PU/PPG-NIPUs discs, using non-activated partial thromboplastin time (NaPTT) testing (**Figure 5.C**). PPP alone was used as CTL -, while kaolin-coated glass coverslips were used as CTL + of coagulation activation. Plasma incubation with PU led to a mean clotting time of 180 s. Among tested NIPUs (PPG-NIPU SH2, PPG-NIPU SH3 and PPG-NIPU SH4), PPG-NIPU SH2 showed longer clotting times (mean value of 303 s) than PU ($p < 0.001$), indicating some superiority of this NIPU over the two others in terms of preventing contact activation. Prolonged clotting times often correlate with improved thromboresistance of the biomaterial [78] and different authors describe longer clotting times for modified/coated PUs. For instance, Zheng *et al*. [79] showed a statistically significant increase in plasma clotting times when comparing pristine PU surfaces with Gastrodin/PU, suggesting the enhanced anti-coagulation nature of Gastrodin by delaying intrinsic pathways. According to our results, NIPUs also appear to have a more interesting anti-thrombogenic behavior than PU when it comes to contact activation of plasma coagulation. Applications of these NIPU-based biomaterials for blood-contacting implants and prostheses with application in the cardiovascular system is therefore very promising.

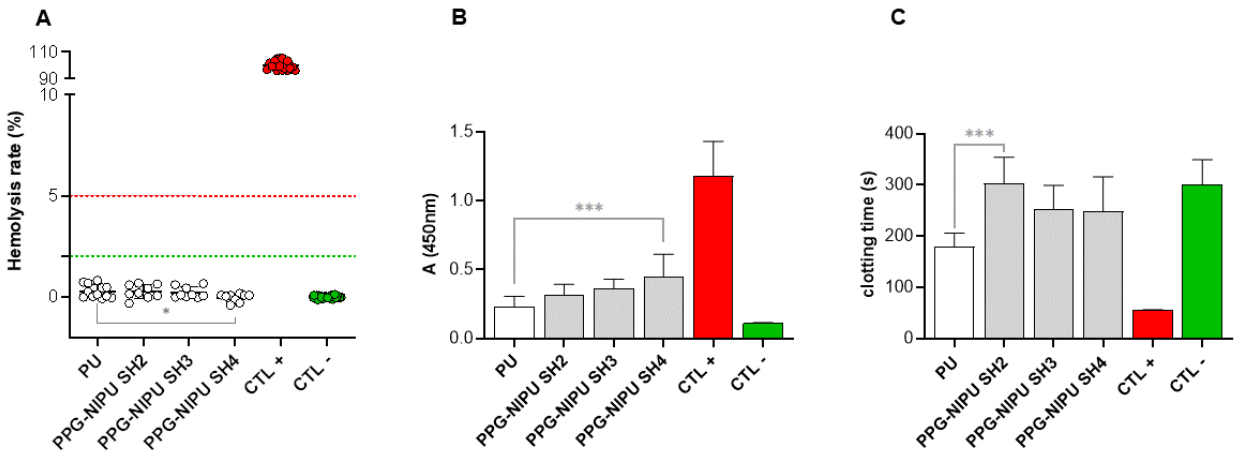

Figure 5: Hemolysis rate in RBCs after 3 h of direct contact with PU/PPG-NIPU discs, assessed by absorbance measurements in the supernatants (A). LDH activity of adhered human platelets after 2 h of direct contact with PU/PPG-NIPU discs, assessed by a colorimetric assay (B). Clotting endpoint times of PPP after 2 h of direct contact with PU/PPG-NIPU discs (C). Statistically significant differences between PU and NIPUs were

computed using one-way ANOVA (*: adjusted p value ≤ 0.05; ***: adjusted p value < 0.001).

Conclusion

New elastomeric biomaterials were prepared based on a poly(propylene glycol) polyhydroxyurethane (PPG-PHU) in which the hydroxyl groups were successfully quantitatively functionalized by an αCC carrying a pendant unsaturation and synthesized starting from CO_2. The subsequent thiol-ene reaction between these unsaturations and various polythiols allowed the photo-crosslinking of this polymer into PPG-NIPU networks exhibiting remarkable thermal, mechanical, and biological properties. The impact of the polythiols used on the thermo-mechanical properties of the final materials was demonstrated by DSC and DMA experiments and showed values suitable for several biomedical applications, such as synthetic vascular grafts or heart valve prostheses. Rheology experiments demonstrated the compatibility of the different formulations with light-based 3D-printing processes. Small objects were then 3D-printed by DLP, proving the future possibility to customize parts of biomedical devices or implants after further optimization of print parameters. Finally, the *in vitro* bio/hemocompatibility tests, performed upon contact between the materials and human fibroblasts, red blood cells, human platelets, or platelet-poor plasma, showed NIPUs bio- and hemocompatible profiles, proving the suitability of these materials to be used in a biomedical context, including as blood-contacting implants.

Conflict of interest

There are no conflicts of interest to declare.

Author Contributions

Anna Pierrard‡: Conceptualization, Formal analysis (Synthesis, Properties of the networks, Rheological measurements and 3D printing), Investigation and Writing-Original Draft. Sofia F. Melo‡: Conceptualization, Formal analysis (Biological tests), Investigation and Writing-Original Draft. Quinten Thijssen: Formal analysis (3D printing). Sandra Van Vlierberghe: Reviewing. Patrizio Lancellotti: Supervision. Cécile Oury: Supervision, Writing-Reviewing and Editing. Christophe Detrembleur: Supervision, Writing-Reviewing

and Editing. Christine Jérôme: Supervision, Writing-Reviewing and Editing. ‡Authors contributed equally to this work.

Acknowledgements

The authors would like to acknowledge the funding from "Fonds Wetenschappelijk Onderzoek" FWO (FWO-SB fellow - 1SA2321N) and the "Fonds de la Recherche Scientifique" F.R.S.-FNRS in the frame of the FRIA grant of S. F. Melo and the Research Director positions of C.D. and C.O.. S. F. Melo obtained additional financial support from the GIGA Doctoral School for Health Sciences and the "Fondation Léon Frédéricq". C.D. thanks FNRS for financing the CO_2Switch project (convention T.0075.20).

Associated Content

Supporting Information

Supplementary data can be found in electronic supplementary information (ESI) (PDF): Synthesis of PPG-PHU and its precursors, synthesis of αCC, ^{1}H- and HSQC-NMR spectra of PPG-PHU and αCC-PPG-PHU, FTIR-ATR spectra and SEC chromatograms of PPG-PHU and αCC-PPG-PHU, ^{1}H-NMR and FTIR-ATR spectra of αCC, FTIR-ATR spectra of the PPG-NIPU networks formed with SH2, SH3 and SH4, DSC and TGA curves of PPG-PHU, αCC-PPG-PHU and the PPG-NIPU networks formed with SH2, SH3 and SH4, Viscosity as a function of shear rate for the formulation with SH3 in NMP, CAD model for DLP and optical microscopy images of 3D printed samples, table of the theoretical and experimentally determined sizes of the printed objects.

Bibliography

(1) Rokicki, G.; Parzuchowski, P. G.; Mazurek, M. Non-Isocyanate Polyurethanes : Synthesis , Properties , and Applications. *Polym. Adv. Technol.* **2015**, *26*, 707–761. https://doi.org/10.1002/pat.3522.

(2) Cornille, A.; Auvergne, R.; Figovsky, O.; Boutevin, B.; Caillol, S. A Perspective Approach to Sustainable Routes for Non-Isocyanate Polyurethanes. *Eur. Polym. J.* **2017**, *87*, 535–552. https://doi.org/10.1016/j.eurpolymj.2016.11.027.

(3) Xie, F.; Zhang, T.; Bryant, P.; Kurusingal, V.; Colwell, J. M.; Laycock, B. Degradation and Stabilization of Polyurethane Elastomers. *Progress in Polymer Science* **2019**, *90*, 211–268. https://doi.org/10.1016/j.progpolymsci.2018.12.003.

(4) Lowinger, M.; Barrett, S.; Zhang, F.; Williams, R. Sustained Release Drug Delivery Applications of Polyurethanes. *Pharmaceutics* **2018**, *10* (2), 55. https://doi.org/10.3390/pharmaceutics10020055.

(5) Salimi, S.; Wu, Y.; Barreiros, M. I. E.; Natfji, A. A.; Khaled, S.; Wildman, R.; Hart, L. R.; Greco, F.; Clark, E. A.; Roberts, C. J.; Hayes, W. A 3D Printed Drug Delivery Implant Formed from a Dynamic Supramolecular Polyurethane Formulation. *Polym. Chem.* **2020**, *11* (20), 3453–3464. https://doi.org/10.1039/D0PY00068J.

(6) Penhasi, A.; Gertler, A.; Baluashvili, I.; Elzinaty, O.; Shalev, D. E. High Modulus Thermoplastic Segmented Polyurethane/Poly(L-lactide) Blends as Potential Candidates for Structural Implantable Drug Delivery Systems: I. Structure-properties Relationship Study. *J Appl. Polym. Sci.* **2020**, *137* (36), 49517. https://doi.org/10.1002/app.49517.

(7) Alves, P.; Ferreira, P.; Gil, H. Biomedical Polyurethane-Based Materials. **2012**, *Chapter 1*.

(8) Wendels, S.; Avérous, L. Biobased Polyurethanes for Biomedical Applications. *Bioactive Materials* **2021**, *6* (4), 1083–1106. https://doi.org/10.1016/j.bioactmat.2020.10.002.

(9) IndustryARC. *Medical Polyurethane Market Report - Forecast 2021-2026*. **2023**. https://www.industryarc.com/Report/18850/medical-polyurethane-market.

(10) Fathi-Karkan, S.; Banimohamad-Shotorbani, B.; Saghati, S.; Rahbarghazi, R.; Davaran, S. A Critical Review of Fibrous Polyurethane-Based Vascular Tissue Engineering Scaffolds. *J Biol Eng* **2022**, *16* (1), 6. https://doi.org/10.1186/s13036-022-00286-9.

(11) Gostev, A. A.; Karpenko, A. A.; Laktionov, P. P. Polyurethanes in Cardiovascular Prosthetics. *Polym. Bull.* **2018**, *75* (9), 4311–4325. https://doi.org/10.1007/s00289-017-2266-x.

(12) Gostev, A.; Shundrina, I.; Pastukhov, V.; Shutov, A.; Chernonosova, V.; Karpenko, A.; Laktionov, P. In Vivo Stability of Polyurethane-Based Electrospun Vascular Grafts in Terms of Chemistry and Mechanics. *Polymers* **2020**, *12* (4), 845. https://doi.org/10.3390/polym12040845.

(13) Chandy, T.; Van Hee, J.; Nettekoven, W.; Johnson, J. Long-term *in Vitro* Stability Assessment of Polycarbonate Urethane Micro Catheters: Resistance to Oxidation and Stress Cracking. *J. Biomed. Mater. Res.* **2009**, *89B* (2), 314–324. https://doi.org/10.1002/jbm.b.31218.

(14) Serkis, M.; Špírková, M.; Poręba, R.; Hodan, J.; Kredatusová, J.; Kubies, D. Hydrolytic Stability of Polycarbonate-Based Polyurethane Elastomers Tested in Physiologically Simulated Conditions. *Polymer Degradation and Stability* **2015**, *119*, 23–34. https://doi.org/10.1016/j.polymdegradstab.2015.04.030.

(15) Redlich, C. A.; Karol, M. H. Diisocyanate Asthma : Clinical Aspects and Immunopathogenesis. *International Immunopharmacology* **2002**, *2*, 213–224.

(16) Allport, D. C.; Gilbert, D. S.; Outterside, S. M. MDI and TDI : Safety , Health and the Environment . A Source Book and Practical Guide. *John Wiley & Sons Ltd., Chichester* **2003**.

(17) Lim, S.-C.; Yang, J.-Y.; Jang, A.-S.; Park, Y.-U.; Kim, Y.-C.; Choi, I.-S.; Park, K.-O. Acute Lung Injury after Phosgene Inhalation. *The Korean Journal of Internal Medicine* **1996**, *11* (1), 87–92.

(18) Gutch, M.; Jain, N.; Agrawal, A.; Consul, S. Acute Accidental Phosgene Poisoning. *Case Reports*, **2012**, bcr1120115233, 7–10. https://doi.org/10.1136/bcr.11.2011.5233.

(19) Commission Regulation (EC) No 552/2009 of 22 June 2009 Amending Regulation (EC) No 1907/2006 of the European Parliament and of the Council on the Registration, Evaluation, Authorisation and Restriction of Chemicals (REACH) as Regards Annex XVII. *Official Journal of the European Union* **2009**, L164/7-L164/31.

(20) Gomez-lopez, A.; Elizalde, F.; Calvo, I.; Sardon, H. Trends in Non-Isocyanate Polyurethane (NIPU) Development. *Chem. Commun.* **2021**, *57*, 12254–12265. https://doi.org/10.1039/d1cc05009e.

(21) Maisonneuve, L.; Lamarzelle, O.; Rix, E.; Grau, E.; Cramail, H. Isocyanate-Free Routes to Polyurethanes and Poly(Hydroxy Urethane)s. *Chem. Rev.* **2015**, *115* (22), 12407–12439. https://doi.org/10.1021/acs.chemrev.5b00355.

(22) Kathalewar, M. S.; Joshi, P. B.; Sabnis, A. S.; Malshe, V. C. Non-Isocyanate Polyurethanes : From Chemistry to Applications. *RSC Adv.* **2013**, *3*, 4110–4129. https://doi.org/10.1039/C2RA21938G.

(23) Sardon, H.; Pascual, A.; Mecerreyes, D.; Taton, D.; Cramail, H.; Hedrick, J. L. Synthesis of Polyurethanes Using Organocatalysis : A Perspective. *Macromolecules* **2015**, *48*, 3153–3165. https://doi.org/10.1021/acs.macromol.5b00384.

(24) Stachak, P.; Łukaszewska, I.; Hebda, E.; Pielichowski, K. Recent Advances in Fabrication of Non-Isocyanate Polyurethane-Based Composite Materials. *Materials* **2021**, 14, 3497.

(25) Guan, J.; Song, Y.; Lin, Y.; Yin, X.; Zuo, M.; Zhao, Y.; Tao, X.; Zheng, Q. Progress in Study of Non-Isocyanate Polyurethane. *Industrial and Engineering Chemistry Research* **2011**, *50* (11), 6517–6527. https://doi.org/10.1021/ie101995j.

(26) Grignard, B.; Gennen, S.; Jérôme, C.; Kleij, A. W.; Detrembleur, C. Advances in the Use of CO $_2$ as a Renewable Feedstock for the Synthesis of Polymers. *Chem. Soc. Rev.* **2019**, *48* (16), 4466–4514. https://doi.org/10.1039/C9CS00047J.

(27) Pescarmona, P. P.; Taherimehr, M. Challenges in the Catalytic Synthesis of Cyclic and Polymeric Carbonates from Epoxides and CO2. *Catal. Sci. Technol.* **2012**, *2* (11), 2169. https://doi.org/10.1039/c2cy20365k.

(28) Martín, C.; Fiorani, G.; Kleij, A. W. Recent Advances in the Catalytic Preparation of Cyclic Organic Carbonates. *ACS Catal.* **2015**, *5* (2), 1353–1370. https://doi.org/10.1021/cs5018997.

(29) Alves, M.; Grignard, B.; Mereau, R.; Jerome, C.; Tassaing, T.; Detrembleur, C. Organocatalyzed Coupling of Carbon Dioxide with Epoxides for the Synthesis of Cyclic Carbonates: Catalyst Design and Mechanistic Studies. *Catal. Sci. Technol.* **2017**, *7*, 2651–2684. https://doi.org/10.1039/C7CY00438A.

(30) Büttner, H.; Longwitz, L.; Steinbauer, J.; Wulf, C.; Werner, T. Recent Developments in the Synthesis of Cyclic Carbonates from Epoxides and CO2. *Top Curr Chem (Z)* **2017**, *375* (3), 50. https://doi.org/10.1007/s41061-017-0136-5.

(31) Kamphuis, A. J.; Picchioni, F.; Pescarmona, P. P. CO2 -Fixation into Cyclic and Polymeric Carbonates: Principles and Applications. *Green Chem.* **2019**, *21* (3), 406–448. https://doi.org/10.1039/C8GC03086C.

(32) de la Cruz-Martínez, F.; Martínez de Sarasa Buchaca, M.; Martínez, J.; Fernández-Baeza, J.; Sánchez-Barba, L. F.; Rodríguez-Diéguez, A.; Castro-Osma, J. A.; Lara-Sánchez, A. Synthesis of Bio-Derived Cyclic Carbonates from Renewable Resources. *ACS Sustainable Chem. Eng.* **2019**, *7* (24), 20126–20138. https://doi.org/10.1021/acssuschemeng.9b06016.

(33) Aomchad, V.; Cristòfol, À.; Della Monica, F.; Limburg, B.; D'Elia, V.; Kleij, A. W. Recent Progress in the Catalytic Transformation of Carbon Dioxide into Biosourced Organic Carbonates. *Green Chem.* **2021**, *23* (3), 1077–1113. https://doi.org/10.1039/D0GC03824E.

(34) Ecochard, Y.; Caillol, S. Hybrid Polyhydroxyurethanes : How to Overcome Limitations and Reach Cutting Edge Properties ? *Eur. Polym. J.,* **2020**, *137*, 109915. https://doi.org/10.1016/j.eurpolymj.2020.109915.

(35) Tryznowski, M.; Swiderska, A.; Zolek-Tryznowska, Z.; Golofit, T.; Parzuchowski, P. G. Facile Route to Multigram Synthesis of Environmentally Friendly Non-Isocyanate Polyurethanes. *Polymer* **2015**, *80*, 228–236. https://doi.org/10.1016/j.polymer.2015.10.055.

(36) Beniah, G.; Fortman, D. J.; Heath, W. H.; Dichtel, W. R.; Torkelson, J. M. Non-Isocyanate Polyurethane Thermoplastic Elastomer : Amide- Based Chain Extender Yields Enhanced Nanophase Separation and Properties in Polyhydroxyurethane. *Macromolecules* **2017**, *50*, 4425–4434. https://doi.org/10.1021/acs.macromol.7b00765.

(37) Leitsch, E. K.; Beniah, G.; Liu, K.; Lan, T.; Heath, W. H.; Scheidt, K. A.; Torkelson, J. M. Nonisocyanate Thermoplastic Polyhydroxyurethane Elastomers via Cyclic Carbonate Aminolysis: Critical Role of Hydroxyl Groups in Controlling Nanophase Separation. *ACS Macro Lett.* **2016**, *5*, 424–229. https://doi.org/10.1021/acsmacrolett.6b00102.

(38) Pierrard, A.; Aqil, A.; Detrembleur, C.; Jérôme, C. Thermal and UV Curable Formulations of Poly(Propylene Glycol)–Poly(Hydroxyurethane) Elastomers toward Nozzle-Based 3D Photoprinting. *Biomacromolecules* **2023**, *24* (10), 4375–4384. https://doi.org/10.1021/acs.biomac.2c00860.

(39) Pronoitis, C.; Hakkarainen, M.; Odelius, K. Solubility-Governed Architectural Design of Polyhydroxyurethane-Graft-Poly(ε-Caprolactone) Copolymers. *Polym. Chem.* **2021**, *12*, 196–208. https://doi.org/10.1039/d0py01089h.

(40) Pramanik, S. K.; Sreedharan, S.; Singh, H.; Khan, M.; Tiwari, K.; Shiras, A.; Smythe, C.; Thomas, Jim. A.; Das, A. Mitochondria Targeting Non-Isocyanate-Based Polyurethane Nanocapsules for Enzyme-Triggered Drug Release. *Bioconjugate Chem.* **2018**, *29* (11), 3532–3543. https://doi.org/10.1021/acs.bioconjchem.8b00460.

(41) Esmaeili, N.; Zohuriaan-Mehr, M. J.; Salimi, A.; Vafayan, M.; Meyer, W. Tannic Acid Derived Non-Isocyanate Polyurethane Networks: Synthesis, Curing Kinetics,

Antioxidizing Activity and Cell Viability. *Thermochimica Acta* **2018**, *664*, 64–72. https://doi.org/10.1016/j.tca.2018.04.013.

(42) Warner, J. J.; Wang, P.; Mellor, W. M.; Hwang, H. H.; Park, J. H.; Pyo, S.-H.; Chen, S. 3D Printable Non-Isocyanate Polyurethanes with Tunable Material Properties. *Polym. Chem.* **2019**, *10* (34), 4665–4674. https://doi.org/10.1039/C9PY00999J.

(43) Pyo, S.-H.; Wang, P.; Hwang, H. H.; Zhu, W.; Warner, J.; Chen, S. Continuous Optical 3D Printing of Green Aliphatic Polyurethanes. *ACS Appl. Mater. Interfaces* **2017**, *9* (1), 836–844. https://doi.org/10.1021/acsami.6b12500.

(44) Fanjul-Mosteirín, N.; Aguirresarobe, R.; Sadaba, N.; Larrañaga, A.; Marin, E.; Martin, J.; Ramos-Gomez, N.; Arno, M. C.; Sardon, H.; Dove, A. P. Crystallization-Induced Gelling as a Method to 4D Print Low-Water-Content Non-Isocyanate Polyurethane Hydrogels. *Chem. Mater.* **2021**, *33* (18), 7194–7202. https://doi.org/10.1021/acs.chemmater.1c00913.

(45) Aduba, D. C.; Zhang, K.; Kanitar, A.; Sirrine, J. M.; Verbridge, S. S.; Long, T. E. Electrospinning of Plant Oil-based, Non-isocyanate Polyurethanes for Biomedical Applications. *J. Appl. Polym. Sci.* **2018**, No. 46464, 1–11. https://doi.org/10.1002/app.46464.

(46) Zhao, Y.; Xia, X.; Zhou, J.; Huang, Z.; Lei, F.; Tan, X.; Yu, D.; Zhu, Y.; Xu, H. Thermoresponsive Behavior of Non-Isocyanate Poly(Hydroxyl)Urethane for Biomedical Composite Materials. *Adv Compos Hybrid Mater* **2022**, *5* (2), 843–852. https://doi.org/10.1007/s42114-021-00379-x.

(47) Gennen, S.; Grignard, B.; Tassaing, T.; Jérôme, C.; Detrembleur, C. CO2-Sourced α-Alkylidene Cyclic Carbonates: A Step Forward in the Quest for Functional Regioregular Poly(Urethane)s and Poly(Carbonate)s. *Angewandte Chemie - International Edition* **2017**, *56* (35), 10394–10398. https://doi.org/10.1002/anie.201704467.

(48) Bähr, M.; Mülhaupt, R. Linseed and Soybean Oil-Based Polyurethanes Prepared via the Non-Isocyanate Route and Catalytic Carbon Dioxide Conversion. *Green Chemistry* **2012**, *14* (2), 483–489. https://doi.org/10.1039/c2gc16230j.

(49) Grignard, B.; Ngassamtounzoua, C.; Gennen, S.; Gilbert, B.; Méreau, R.; Jerome, C.; Tassaing, T.; Detrembleur, C. Boosting the Catalytic Performance of Organic Salts for the Fast and Selective Synthesis of α-Alkylidene Cyclic Carbonates from Carbon Dioxide and Propargylic Alcohols. *ChemCatChem* **2018**, *10* (12), 2584–2592. https://doi.org/10.1002/cctc.201800063.

(50) Ngassam Tounzoua, C.; Grignard, B.; Detrembleur, C. Exovinylene Cyclic Carbonates : Multifaceted CO2 -Based Building Blocks for Modern Chemistry and Polymer Science. *Angew. Chem. Int. Ed.* **2022**, *61* (e202116066), 1–25. https://doi.org/10.1002/anie.202116066.

(51) Siragusa, F.; Van Den Broeck, E.; Ocando, C.; Müller, A. J.; De Smet, G.; Maes, B. U. W.; De Winter, J.; Van Speybroeck, V.; Grignard, B.; Detrembleur, C. Access to Biorenewable and CO 2 - Based Polycarbonates from Exovinylene Cyclic Carbonates. *ACS Sustainable Chem. Eng.* **2021**, *9*, 1714–1728. https://doi.org/10.1021/acssuschemeng.0c07683.

(52) Monie, F.; Grignard, B.; Detrembleur, C. Divergent Aminolysis Approach for Constructing Recyclable Self-Blown Nonisocyanate Polyurethane Foams. *ACS Macro Lett.* **2022**, *11* (2), 236–242. https://doi.org/10.1021/acsmacrolett.1c00793.

(53) Pronoitis, C.; Hakkarainen, M.; Odelius, K. Structurally Diverse and Recyclable Isocyanate-Free Polyurethane Networks from CO2-Derived Cyclic Carbonates. *ACS Sustainable Chemistry & Engineering* **2022**, *10*, 2522–2531. https://doi.org/10.1021/acssuschemeng.1c08530.

(54) Bourguignon, M.; Grignard, B.; Detrembleur, C. Water-Induced Self-Blown Non-Isocyanate Polyurethane Foams. *Angew. Chem. Int. Ed.* **2022**, *61*, e202213422. https://doi.org/doi.org/10.1002/anie.202213422.

(55) Choong, P. S.; Chong, N. X.; Wai Tam, E. K.; Seayad, A. M.; Seayad, J.; Jana, S. Biobased Nonisocyanate Polyurethanes as Recyclable and Intrinsic Self-Healing Coating with Triple Healing Sites. *ACS Macro Lett.* **2021**, *10* (5), 635–641. https://doi.org/10.1021/acsmacrolett.1c00163.

(56) McKenna, K. A.; Hinds, M. T.; Sarao, R. C.; Wu, P.-C.; Maslen, C. L.; Glanville, R. W.; Babcock, D.; Gregory, K. W. Mechanical Property Characterization of Electrospun Recombinant Human Tropoelastin for Vascular Graft Biomaterials. *Acta Biomaterialia* **2012**, *8* (1), 225–233. https://doi.org/10.1016/j.actbio.2011.08.001.

(57) King III, W. E.; Minden-Birkenmaier, B. A.; Bowlin, G. L. Synthetic Materials: Processing and Surface Modifications for Vascular Tissue Engineering. In *Tissue-Engineered Vascular Grafts*; Walpoth, B. H., Bergmeister, H., Bowlin, G. L., Kong, D., Rotmans, J. I., Zilla, P., Eds.; Springer International Publishing: Cham, 2020; pp 1–50. https://doi.org/10.1007/978-3-030-05336-9.

(58) Hasan, A.; Ragaert, K.; Swieszkowski, W.; Selimović, Š.; Paul, A.; Camci-Unal, G.; Mofrad, M. R. K.; Khademhosseini, A. Biomechanical Properties of Native and Tissue Engineered Heart Valve Constructs. *Journal of Biomechanics* **2014**, *47* (9), 1949–1963. https://doi.org/10.1016/j.jbiomech.2013.09.023.

(59) Balguid, A.; Rubbens, M. P.; Mol, A.; Bank, R. A.; Bogers, A. J. J. C.; van Kats, J. P.; de Mol, B. A. J. M.; Baaijens, F. P. T.; Bouten, C. V. C. The Role of Collagen Cross-Links in Biomechanical Behavior of Human Aortic Heart Valve Leaflets—Relevance for Tissue Engineering. *Tissue Engineering* **2007**, *13* (7), 1501–1511. https://doi.org/10.1089/ten.2006.0279.

(60) Fung, Y. C. Blood Flow in Arteries. In *Biodynamics: Circulation*; Fung, Y. C., Ed.; Springer New York: New York, NY, 1984; pp 77–165. https://doi.org/10.1007/978-1-4757-3884-1_3.

(61) Camasão, D. B.; Mantovani, D. The Mechanical Characterization of Blood Vessels and Their Substitutes in the Continuous Quest for Physiological-Relevant Performances. A Critical Review. *Materials Today Bio* **2021**, *10*, 100106. https://doi.org/10.1016/j.mtbio.2021.100106.

(62) Mea, H.; Wan, J. Microfluidics-Enabled Functional 3D Printing. *Biomicrofluidics* **2022**, *16* (2), 021501. https://doi.org/10.1063/5.0083673.

(63) Thijssen, Q.; Parmentier, L.; Augustyniak, E.; Mouthuy, P.-A.; Van Vlierberghe, S. From Chain Growth to Step Growth Polymerization of Photoreactive Poly-ε-Caprolactone: The Network Topology of Bioresorbable Networks as Tool in Tissue Engineering. *Adv. Funct. Mater.* **2022**, *32*, 2108869. https://doi.org/DOI: 10.1002/adfm.202108869.

(64) Kuhnt, T.; Morgan, F. L. C.; Baker, M. B.; Moroni, L. An Efficient and Easily Adjustable Heating Stage for Digital Light Processing Set-Ups. *Additive Manufacturing* **2021**, *46*, 102102. https://doi.org/10.1016/j.addma.2021.102102.

(65) U.S. Department of Health and Human Services Food and Drug Administration Center for Drug Evaluation and Research (CDER) Center for Biologics Evaluation and Research (CBER), *Q3C — Tables and List Guidance for Industry*, **2017**. https://www.fda.gov/media/71737/download.

(66) Brown, J. A.; Lee, J. H.; Smith, M. A.; Wells, D. R.; Barrett, A.; Puelz, C.; Vavalle, J. P.; Griffith, B. E. Patient–Specific Immersed Finite Element–Difference Model of Transcatheter Aortic Valve Replacement. *Ann Biomed Eng* **2023**, *51* (1), 103–116. https://doi.org/10.1007/s10439-022-03047-3.

(67) *ISO 10993-5:2009 - Biological evaluation of medical devices — Part 5: Tests for in vitro cytotoxicity,* **2009**, 1-34.

(68) Calvo-Correas, T.; Gabilondo, N.; Alonso-Varona, A.; Palomares, T.; Corcuera, M. A.; Eceiza, A. Shape-Memory Properties of Crosslinked Biobased Polyurethanes. *European Polymer Journal* **2016**, *78*, 253–263. https://doi.org/10.1016/J.EURPOLYMJ.2016.03.030.

(69) Valdés, B. S. G.; Gomes, C. S. B.; Gomes, P. T.; Ascenso, J. R.; Diogo, H. P.; Gonçalves, L. M.; dos Santos, R. G.; Ribeiro, H. M.; Bordado, J. C. Synthesis and Characterization of Isosorbide-Based Polyurethanes Exhibiting Low Cytotoxicity Towards HaCaT Human Skin Cells. *Polymers* **2018**, 10 (10), 1170. https://doi.org/10.3390/POLYM10101170.

(70) Ward, R.S.; Jones, R.L. 1.26 Polyurethanes and Silicone Polyurethane Copolymers. (In Comprehensive Biomaterials II). *Reference Module in Materials Science and Materials Engineering*; **2017**, 570–619. https://doi.org/10.1016/B978-0-08-100691-7.00179-8.

(71) Wang, W.; Wang, C. Polyurethane for Biomedical Applications: A Review of Recent Developments. In *The Design and Manufacture of Medical Devices*; Elsevier, 2012; pp 115–151. https://doi.org/10.1533/9781908818188.115.

(72) Shelke, N. B.; Nagarale, R. K.; Kumbar, S. G. Polyurethanes. In *Natural and Synthetic Biomedical Polymers*; Elsevier, 2014; pp 123–144. https://doi.org/10.1016/B978-0-12-396983-5.00007-7.

(73) Bonfil, M.; Sirkecioglu, A.; Bingol-Ozakpinar, O.; Uras, F.; Güner, F. S. Castor Oil and PEG-Based Shape Memory Polyurethane Films for Biomedical Applications. *J. Appl. Polym. Sci.* **2014**, *131* (15), 40590. https://doi.org/10.1002/APP.40590.

(74) Duarah, R.; Singh, Y. P.; Mandal, B. B.; Karak, N. Sustainable Starch Modified Polyol Based Tough, Biocompatible, Hyperbranched Polyurethane with a Shape Memory Attribute. *New Journal of Chemistry* **2016**, *40* (6), 5152–5163. https://doi.org/10.1039/C5NJ03294F.

(75) Standard Practice for Assessment of Hemolytic Properties of Materials. *ASTM F756-00*, **2010**, 13.01, 1-5. https://doi.org/10.1520/F0756-00.

(76) Mystkowska, J.; Mazurek-Budzyńska, M.; Piktel, E.; Niemirowicz, K.; Karalus, W.; Deptuła, P.; Pogoda, K.; Łysik, D.; Dąbrowski, J. R.; Rokicki, G.; Bucki, R. Assessment of Aliphatic Poly(Ester-Carbonate-Urea-Urethane)s Potential as Materials for Biomedical

Application. *Journal of Polymer Research* **2017**, *24* (9), 1–11. https://doi.org/10.1007/S10965-017-1296-2/FIGURES/6.

(77) Zhu, R.; Wang, Y.; Zhang, Z.; Ma, D.; Wang, X. Synthesis of Polycarbonate Urethane Elastomers and Effects of the Chemical Structures on Their Thermal, Mechanical and Biocompatibility Properties. *Heliyon* **2016**, *2* (6), e00125. https://doi.org/10.1016/J.HELIYON.2016.E00125.

(78) Motlagh, D.; Yang, J.; Lui, K. Y.; Webb, A. R.; Ameer, G. A. Hemocompatibility Evaluation of Poly(Glycerol-Sebacate) in Vitro for Vascular Tissue Engineering. *Biomaterials* **2006**, *27* (24), 4315–4324. https://doi.org/10.1016/j.biomaterials.2006.04.010.

(79) Zheng, M.; Guo, J.; Li, Q.; Yang, J.; Han, Y.; Yang, H.; Yu, M.; Zhong, L.; Lu, D.; Li, L.; Sun, L. Syntheses and Characterization of Anti-Thrombotic and Anti-Oxidative Gastrodin-Modified Polyurethane for Vascular Tissue Engineering. *Bioactive Materials* **2021**, *6* (2), 404–419. https://doi.org/10.1016/j.bioactmat.2020.08.008.